

RIS Partitioning Based Scalable Beamforming Design for Large-Scale MIMO: Asymptotic Analysis and Optimization

Chang Cai, *Student Member, IEEE*, Xiaojun Yuan, *Senior Member, IEEE*,
Ying-Jun Angela Zhang, *Fellow, IEEE*

Abstract

In next-generation wireless networks, reconfigurable intelligent surface (RIS)-assisted multiple-input multiple-output (MIMO) systems are foreseeable to support a large number of antennas at the transceiver as well as a large number of reflecting elements at the RIS. To fully unleash the potential of RIS, the phase shifts of RIS elements should be carefully designed, resulting in a high-dimensional non-convex optimization problem that is hard to solve with affordable computational complexity. In this paper, we address this scalability issue by partitioning RIS into sub-surfaces, so as to optimize the phase shifts in sub-surface levels to reduce complexity. Specifically, each sub-surface employs a linear phase variation structure to anomalously reflect the incident signal to a desired direction, and the sizes of sub-surfaces can be adaptively adjusted according to channel conditions. We formulate the achievable rate maximization problem by jointly optimizing the transmit covariance matrix and the RIS phase shifts. Under the RIS partitioning framework, the RIS phase shifts optimization reduces to the manipulation of the sub-surface sizes, the phase gradients of sub-surfaces, as well as the common phase shifts of sub-surfaces. Then, we characterize the asymptotic behavior of the system with an infinitely large number of transceiver antennas and RIS elements. The asymptotic analysis provides useful insights on the understanding of the fundamental performance-complexity tradeoff in RIS partitioning design. We show that the achievable rate maximization problem has a rather simple form with an explicit physical meaning of optimization variables. We develop an efficient algorithm to find the optimal solution to the asymptotic problem via one-dimensional (1D) search. Moreover, we discuss the insights and impacts of the asymptotically optimal solution on finite-size system design. By applying the asymptotic result to a finite-size system with necessary modifications, we show by numerical results that the proposed design achieves a favorable tradeoff between system performance and computational complexity.

Chang Cai and Ying-Jun Angela Zhang are with the Department of Information Engineering, The Chinese University of Hong Kong, Hong Kong (e-mail: cc021@ie.cuhk.edu.hk; yjzhang@ie.cuhk.edu.hk).

Xiaojun Yuan is with the National Key Laboratory of Science and Technology on Communications, University of Electronic Science and Technology of China, Chengdu 611731, China (e-mail: xjyuan@uestc.edu.cn).

Index Terms

Reconfigurable intelligent surface (RIS), RIS partitioning, scalable beamforming design, asymptotic analysis

I. INTRODUCTION

Emerging data-intensive applications, such as virtual reality, holographic projection, and autonomous driving, give rise to urgent needs for high-speed and seamless data services in future wireless systems [1]. A main bottleneck for the improvement of the quality of service (QoS) lies in the randomness and uncontrollability of wireless communication environments, in which the reliability of a link may severely deteriorate due to deep fading and shadowing effects. Thanks to the recent advances on programmable metamaterials [2], [3], reconfigurable intelligent surface (RIS) has emerged as a promising new technology to improve the link reliability of wireless networks as it can artificially configure the wireless channel in a favorable manner. Typically, a RIS is a planar surface consisting of a large number of low-cost and passive reflecting elements. By inducing an appropriately designed phase shift at each passive element, a RIS can manipulate the incident signals to be constructively or destructively superimposed at receiver (Rx) (referred to as *passive beamforming*), thereby reshaping the wireless channel to boost the performance of communication systems [4]–[6].

Extensive research efforts [7]–[17] have been devoted to the optimization of passive beamforming based on various design criteria for RIS-aided communication systems. Aiming to maximize the achievable rate, the joint optimization of transmit beamforming and RIS phase shifts (referred to as *joint active and passive beamforming*) are considered for multiple-input single-output (MISO) systems in [7]–[9] and for multiple-input multiple-output (MIMO) systems in [10], [11]. Ref. [12] developed a RIS power consumption model to study the energy efficiency maximization problem, which shows that a passive RIS is more energy efficient than an amplify-and-forward (AF) relay. Thanks to its ability to suppress interference, RIS is also widely exploited in cognitive radio networks [13], device-to-device (D2D) communications [14], and non-orthogonal multiple access (NOMA) [15]. Moreover, the authors in [16] demonstrated the effectiveness of RIS on improving the over-the-air federated learning (FL) performance.

The passive beamforming design mentioned above, however, faces a serious scalability issue in real implementation. On one hand, the transmitter-RIS-receiver (Tx-RIS-Rx) link suffers from the *double fading effect*, i.e., the equivalent path loss of the Tx-RIS-Rx link is the product

(instead of the sum) of the path losses of the Tx-RIS and RIS-Rx links [18]. The double fading effect results in severe path loss of the Tx-RIS-Rx link. Thus, to achieve a substantial passive beamforming gain, a large RIS with hundreds and thousands of reflecting elements is needed. On the other hand, due to the non-convex unit-modulus constraint imposed on RIS phase shifts, the computational complexity involved in passive beamforming optimization is at least cubic in the number of RIS elements [7]–[17]. This implies a prohibitively high computational complexity even for a RIS with a typical size, which may seriously impede the widespread application of the RIS technology in next-generation wireless communications.

To address the scalability issue, [19]–[24] proposed to partition a RIS into sub-surfaces, where each sub-surface consists of a number of adjacent reflecting elements. Specifically, the authors in [19]–[21] assumed a common phase shift of elements in each sub-surface, thereby reducing the number of passive beamforming variables to that of the sub-surfaces. More recently, the authors in [22], [23] considered a linear phase variation structure in sub-surfaces, where a phase gradient and a common phase shift of each sub-surface can be adjusted for passive beamforming. By employing the linear phase variation structure, a sub-surface can work as an anomalous reflector to change the direction and wavefront of the reflected beam. Clearly, RIS partitioning exhibits a tradeoff between passive beamforming gain and computational complexity, which can be flexibly controlled by adjusting the number of partitioned sub-surfaces. However, the existing approaches in [19]–[24] are all based on heuristic optimization methods that provide limited insights into the utmost potential of the RIS partitioning technique. As such, it is of pressing importance to develop an analytical framework to characterize the fundamental performance-complexity tradeoff of RIS partitioning, which motivates the work presented in this paper.

In this paper, we study joint active and passive beamforming to maximize the achievable rate of the RIS-aided large-scale MIMO system. We take the RIS partitioning approach and provide a scalable solution to the problem of joint active and passive beamforming design. In our RIS partitioning design, each sub-surface adopts a linear phase variation structure to achieve anomalous reflection, and the size of each sub-surface can be adaptively adjusted based on channel conditions. The RIS optimization then reduces to the manipulation of the sub-surface sizes, the phase gradients of sub-surfaces, as well as the common phase shifts of sub-surfaces. Different from the existing works [19]–[24], we focus on the asymptotic regime where the number of RIS reflecting elements and the number of transceiver antennas go to infinity. In this regime, the RIS and the transceiver arrays have infinitely high resolution to distinguish the

Tx-RIS and RIS-Rx channel paths with different arrival and departure angles. We show that the Tx-RIS-Rx channel paths are asymptotically orthogonal to each other, implying that arbitrary common phase shifts of the sub-surfaces are optimal in the asymptotic regime. Based on that, we establish the asymptotic form of the rate maximization problem involving the sub-surface sizes, the phase gradients of sub-surfaces, and the power allocation among different channel paths at the Tx side.

We establish the analytical solution to the above asymptotic rate maximization problem. Specifically, by adopting the linear phase variation structure, each sub-surface needs to reflect the incident signals from a Tx-RIS arrival path to a RIS-Rx departure path, or in other words, the optimization of the sub-surface phase gradients reduces to a Tx-RIS-Rx path pairing problem. We show that the optimal path pairing strategy can be expressed in closed form. Furthermore, by analysing the Karush-Kuhn-Tucker (KKT) conditions of the problem, we show that the global optimum of the RIS partition sizes and the Tx power allocation can be found by one-dimensional (1D) exhaustive search. Interestingly, the optimal RIS partitioning strategy allows for a water-filling-like interpretation. That is, the RIS is dedicated to serving the strongest Tx-RIS and RIS-Rx path pair in the low signal-to-noise (SNR) regime, and is evenly partitioned to serve every paired Tx-RIS-Rx path in the high SNR regime.

We further discuss the insights and impacts of the above asymptotically optimal solution on finite-size system design. We first discuss how to adapt the asymptotic solution to a finite-size system with practical antenna and RIS settings. Then, we show that the proposed RIS partitioning approach only has a marginal performance loss compared to the conventional element-wise optimization method [11], whereas the former reduces the computational time by orders of magnitudes especially when the number of RIS elements is large. Therefore, our proposed RIS partitioning approach strikes an appealing balance between performance and complexity, and provides a scalable solution to the design of large-scale RIS-aided systems.

The rest of this paper is organized as follows. Section II describes the system model of the RIS-aided large-scale MIMO communication with RIS partitioning, and then formulates the achievable rate maximization problem. Section III derives the asymptotic formulation of the problem. Section IV elaborates the algorithm to obtain the asymptotically optimal solution, and then discusses the method to construct a feasible solution for finite-size systems. Section V provides the simulation results. Finally, we conclude this paper in Section VI.

Notations: Lower-case letters are used to denote scalars. Vectors and matrices are denoted

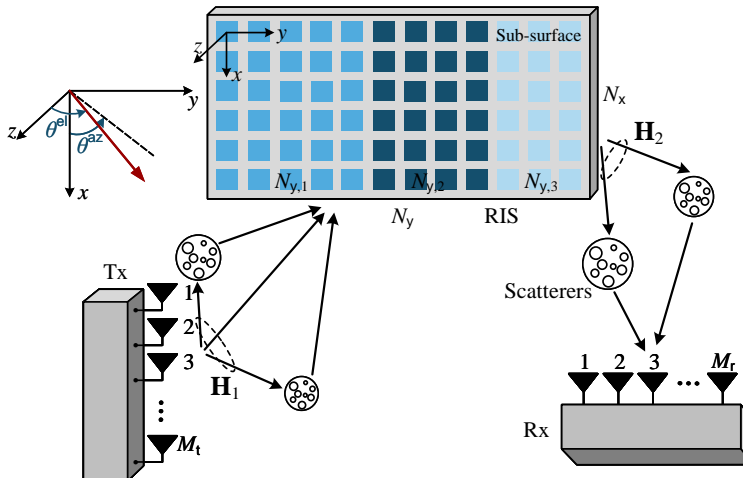


Fig. 1. A RIS-aided large-scale MIMO system. The direct link from the Tx to the Rx is not sketched for clarity of presentation.

by lower-case and upper-case boldface letters, respectively. \mathbf{A}^T , \mathbf{A}^H , \mathbf{A}^{-1} , and $a_{i,j}$ denote the transpose, conjugate transpose, inverse, and (i, j) -th entry of matrix \mathbf{A} , respectively. We use $j \triangleq \sqrt{-1}$, \otimes , $\text{diag}\{\cdot\}$, $\mathbb{E}(\cdot)$, and $\text{tr}(\cdot)$ to represent the imaginary unit, the Kronecker product, the diagonal operator, the expectation operator, and the trace of square matrix, respectively. In addition, $\lfloor \cdot \rfloor$ returns the largest integer that is smaller than or equal to its argument, and $\text{mod}(a, b)$ returns the remainder of the division a/b . We use \mathbb{Z}_+ to denote the set of positive integers. Finally, the distribution of a circularly symmetric complex Gaussian (CSCG) random vector with mean $\boldsymbol{\mu}$ and covariance matrix $\boldsymbol{\Sigma}$ is denoted by $\mathcal{CN}(\boldsymbol{\mu}, \boldsymbol{\Sigma})$; and \sim stands for “distributed as”.

II. RIS-AIDED LARGE-SCALE MIMO SYSTEM

A. System Model

Consider a RIS-aided large-scale MIMO system with M_t transmit antennas and M_r receive antennas ($M_t, M_r \gg 1$), as illustrated in Fig. 1. We assume uniform linear arrays (ULAs) at the Tx and the Rx. A RIS is placed in the three-dimensional (3D) Cartesian coordinate system, where the RIS reflecting elements are arranged in a uniform rectangular array (URA) in the x - y plane with N_x elements in the x -(vertical) axis and N_y elements in the y -(horizontal) axis. Following [7]–[12], the magnitudes of the reflection coefficients are assumed to be a constant. Without loss of generality, the reflection coefficient matrix of the RIS is given by $\boldsymbol{\Theta} = \text{diag}\{e^{j\theta_1}, \dots, e^{j\theta_N}\} \in \mathbb{C}^{N \times N}$, where $N = N_x \times N_y$ is the number of reflecting elements, and θ_n is the phase shift of the n -th reflecting element, $n \in \mathcal{N} \triangleq \{1, \dots, N\}$. We propose to horizontally partition

the RIS into S sub-surfaces, each containing $N_s = N_x \times N_{y,s}$ elements, where $N_{y,s} = t_s N_y$ denotes the number of columns of the RIS array allocated to sub-surface s with partition ratio $t_s \in [0, 1]$, $s \in \mathcal{S} \triangleq \{1, \dots, S\}$. Then, appropriate RIS partitioning can be found by optimizing $\mathbf{t} = [t_1, \dots, t_S]^T$ under the constraints $\sum_{s \in \mathcal{S}} t_s = 1$ and $N_{y,s} \in \mathbb{Z}_+$, $\forall s \in \mathcal{S}$.

We assume that the Tx, the Rx, and the RIS are all deployed in the far-field region of each other, and that the wireless channels are characterized by the ray-tracing based geometric channel model [25]. For ease of notation, we define the following normalized steering vector as a function of angle ϕ and integer M as

$$\mathbf{e}(\phi, M) = \frac{1}{\sqrt{M}} [1, e^{-j\pi\phi}, \dots, e^{-j\pi(M-1)\phi}]^H \in \mathbb{C}^M. \quad (1)$$

The array response of a ULA with M elements is expressed as

$$\mathbf{a}_M(\theta) = \mathbf{e}\left(\frac{2d}{\lambda} \sin \theta, M\right), \quad (2)$$

where θ denotes the angle relative to the antenna boresight, λ denotes the carrier wavelength, and d stands for the element spacing between two adjacent antennas/elements. The RIS array response is expressed as the Kronecker product of two steering vectors in the vertical and horizontal directions, i.e.,

$$\mathbf{b}_N(\theta^{\text{el}}, \theta^{\text{az}}) = \mathbf{e}\left(\frac{2d}{\lambda} \sin \theta^{\text{el}} \cos \theta^{\text{az}}, N_x\right) \otimes \mathbf{e}\left(\frac{2d}{\lambda} \sin \theta^{\text{el}} \sin \theta^{\text{az}}, N_y\right), \quad (3)$$

where θ^{el} and θ^{az} denote the elevation and azimuth angles defined in the 3D Cartesian coordinate system (as shown in Fig. 1), respectively. Based on the notations defined above, the baseband equivalent channel from the Tx to the RIS and from the RIS to the Rx, denoted by $\mathbf{H}_1 \in \mathbb{C}^{N \times M_t}$ and $\mathbf{H}_2 \in \mathbb{C}^{M_r \times N}$ respectively, are expressed as

$$\mathbf{H}_1 = \sqrt{\frac{NM_t}{L_1}} \sum_{\ell=1}^{L_1} \alpha_\ell \mathbf{b}_N(\phi_\ell^{\text{el}}, \phi_\ell^{\text{az}}) \mathbf{a}_{M_t}^H(\phi_\ell), \quad (4)$$

$$\mathbf{H}_2 = \sqrt{\frac{M_r N}{L_2}} \sum_{\ell=1}^{L_2} \beta_\ell \mathbf{a}_{M_r}(\vartheta_\ell) \mathbf{b}_N^H(\vartheta_\ell^{\text{el}}, \vartheta_\ell^{\text{az}}), \quad (5)$$

where L_1 (or L_2) denotes the number of resolvable paths between the Tx and the RIS (or between the RIS and the Rx), α_ℓ (or β_ℓ) denotes the complex gain of the corresponding ℓ -th path, ϕ_ℓ^{el} (or $\vartheta_\ell^{\text{el}}$) and ϕ_ℓ^{az} (or $\vartheta_\ell^{\text{az}}$) denote the ℓ -th elevation and azimuth AoA (or AoD) associated with the RIS, and ϕ_ℓ (or ϑ_ℓ) represents the ℓ -th AoD (or AoA) associated with the Tx (or Rx). Similarly, the channel $\mathbf{H}_3 \in \mathbb{C}^{M_r \times M_t}$ from the Tx to the Rx is expressed as

$$\mathbf{H}_3 = \sqrt{\frac{M_r M_t}{L_3}} \sum_{\ell=1}^{L_3} \gamma_\ell \mathbf{a}_{M_r}(\varphi_\ell) \mathbf{a}_{M_t}^H(\omega_\ell), \quad (6)$$

where L_3 denotes the number of resolvable paths between the Tx and the Rx, γ_ℓ denotes the complex gain of the corresponding ℓ -th path, and φ_ℓ (or ω_ℓ) represents the ℓ -th AoA (or AoD) associated with the Rx (or Tx). For convenience, we assume that the complex gains, $\{\alpha_\ell\}_{\ell=1}^{L_1}$, $\{\beta_\ell\}_{\ell=1}^{L_2}$, and $\{\gamma_\ell\}_{\ell=1}^{L_3}$, are all arranged in the descending order of their magnitudes. Furthermore, since only a limited number of scatterers exist in the wireless propagation environment, the number of channel paths is usually much smaller than the numbers of the array antennas and the reflecting elements, namely $L_1 \ll \min\{M_t, N\}$, $L_2 \ll \min\{M_r, N\}$, and $L_3 \ll \min\{M_t, M_r\}$.

Based on the system model described above, the received signal vector $\mathbf{y} \in \mathbb{C}^{M_r}$ is given by

$$\mathbf{y} = \mathbf{H}_{\text{eff}}\mathbf{x} + \mathbf{n}, \quad (7)$$

where

$$\mathbf{H}_{\text{eff}} \triangleq \sqrt{\text{PL}^r}\mathbf{H}_2\mathbf{\Theta}\mathbf{H}_1 + \sqrt{\text{PL}^d}\mathbf{H}_3 \quad (8)$$

is the effective MIMO channel matrix from the Tx to the Rx, with PL^r and PL^d being the path losses of the cascaded and Tx-Rx channels, respectively, $\mathbf{x} \in \mathbb{C}^{M_t}$ is the transmitted signal vector with zero mean, i.e., $\mathbb{E}[\mathbf{x}] = 0$, and $\mathbf{n} \sim \mathcal{CN}(\mathbf{0}, \sigma^2\mathbf{I}_{M_r})$ denotes the independent CSCG noise vector at the Rx, with σ^2 being the average noise power. Moreover, the transmit signal covariance matrix is defined as $\mathbf{Q} \triangleq \mathbb{E}[\mathbf{x}\mathbf{x}^H] \in \mathbb{C}^{M_t \times M_t}$, where $\mathbf{Q} \succeq \mathbf{0}$. The power budget is denoted by P , i.e., $\mathbb{E}[\|\mathbf{x}\|^2] \leq P$, or equivalently, $\text{tr}(\mathbf{Q}) \leq P$.

B. Phase-Shift Structure Specification

The RIS partitioning design provides a new paradigm that treats the sub-surfaces instead of individual elements as design entities, thereby reducing the dimension of the optimization space involved in the passive beamforming design. In this paper, we propose to design each sub-surface to reflect the incident signals from an AoA of the Tx-RIS channel to an AoD of the RIS-Rx channel, referred to as *anomalous reflection*. Fig. 2 illustrates the basic idea of the proposed design where the RIS is partitioned into three sub-surfaces, with sub-surface 1 reflecting the signals from the AoA $(\phi_3^{\text{el}}, \phi_3^{\text{az}})$ to the AoD $(\vartheta_1^{\text{el}}, \vartheta_1^{\text{az}})$, sub-surface 2 reflecting the signals from the AoA $(\phi_1^{\text{el}}, \phi_1^{\text{az}})$ to the AoD $(\vartheta_2^{\text{el}}, \vartheta_2^{\text{az}})$, and sub-surface 3 reflecting the signals from the AoA $(\phi_2^{\text{el}}, \phi_2^{\text{az}})$ to the AoD $(\vartheta_3^{\text{el}}, \vartheta_3^{\text{az}})$. According to the generalized Snell's law [2], anomalous reflection can be achieved by setting a linear variation of the phase shifts across the x - y plane. Specifically, for sub-surface s to achieve the anomalous reflection from the incident angle $(\phi_u^{\text{el}}, \phi_u^{\text{az}})$ to the

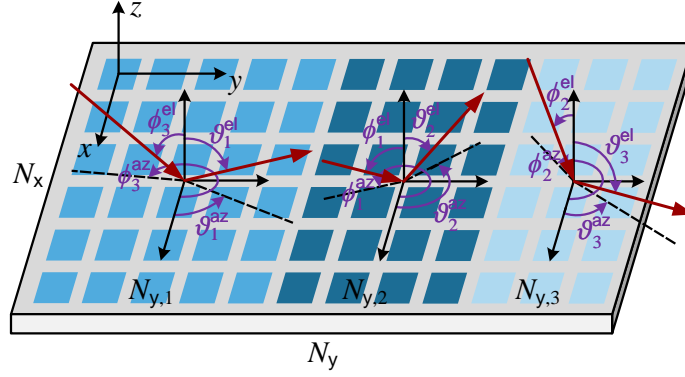


Fig. 2. An illustration of the RIS partitioning design, where the RIS is partitioned into three sub-surfaces with sub-surface 1 serving the AoA $(\phi_3^{el}, \phi_3^{az})$ and the AoD $(\vartheta_1^{el}, \vartheta_1^{az})$, sub-surface 2 serving the AoA $(\phi_1^{el}, \phi_1^{az})$ and the AoD $(\vartheta_2^{el}, \vartheta_2^{az})$, and sub-surface 3 serving the AoA $(\phi_2^{el}, \phi_2^{az})$ and the AoD $(\vartheta_3^{el}, \vartheta_3^{az})$.

reflection angle $(\vartheta_v^{el}, \vartheta_v^{az})$, the phase difference between any two adjacent elements is set to $\frac{2\pi d}{\lambda} g_{x,s}$ along the x -axis, and to $\frac{2\pi d}{\lambda} g_{y,s}$ along the y -axis, respectively, where

$$\mathbf{g}_s \triangleq \begin{bmatrix} g_{x,s} \\ g_{y,s} \end{bmatrix} = \begin{bmatrix} \sin \vartheta_v^{el} \cos \vartheta_v^{az} - \sin \phi_u^{el} \cos \phi_u^{az} \\ \sin \vartheta_v^{el} \sin \vartheta_v^{az} - \sin \phi_u^{el} \sin \phi_u^{az} \end{bmatrix} \quad (9)$$

is referred to as the *phase gradient* of sub-surface s , with $g_{x,s}$ and $g_{y,s}$ being the phase gradient components along the x - and y -axes, respectively, $u \in \mathcal{L}_1 \triangleq \{1, \dots, L_1\}$, and $v \in \mathcal{L}_2 \triangleq \{1, \dots, L_2\}$. The feasible set of the phase gradient \mathbf{g}_s is expressed as

$$\mathcal{F} \triangleq \{ [\zeta_{x,u,v}, \zeta_{y,u,v}]^T \mid u \in \mathcal{L}_1, v \in \mathcal{L}_2 \}, \quad (10)$$

where $\zeta_{x,u,v} \triangleq \sin \vartheta_v^{el} \cos \vartheta_v^{az} - \sin \phi_u^{el} \cos \phi_u^{az}$, and $\zeta_{y,u,v} \triangleq \sin \vartheta_v^{el} \sin \vartheta_v^{az} - \sin \phi_u^{el} \sin \phi_u^{az}$.¹

Remark 1. Although it is crucial for the sub-surfaces to reflect signals along the strong Tx-RIS-Rx paths in order to ensure sufficient link budget, it is unwise to let the sub-surfaces select the strongest Tx-RIS-Rx path all together, i.e., set $\mathbf{g}_s = [\zeta_{x,1,1}, \zeta_{y,1,1}]^T$ for all $s \in \mathcal{S}$. The reason is that the constructed cascaded channel is rank-deficient and thus cannot support multiplexing.

Apart from the phase gradient, a *common phase shift*, denoted as ψ_s , is imposed on every element of sub-surface s , $s \in \mathcal{S}$. That is, the reflection coefficient of the n -th element is given by

$$e^{j\theta_n} = e^{j\psi_s} e^{j\frac{2\pi(n_x-1)d}{\lambda} g_{x,s}} e^{j\frac{2\pi(n_y-1)d}{\lambda} g_{y,s}}, \quad n \in \mathcal{N}, \quad (11)$$

¹We assume that $[\zeta_{x,u,v}, \zeta_{y,u,v}]^T$ has distinct values for different u and/or v . That is, each element in \mathcal{F} is unique.

where $n_x = \lfloor (n-1)/N_x \rfloor + 1$, $n_y = \text{mod}(n-1, N_x) + 1$, and s is the sub-surface index of the n -th reflecting element. In (11), the common phase shift ψ_s adjusts the reflected wavefront, and the phase gradient \mathbf{g}_s determines the direction of the beam reflected by sub-surface s .

C. Problem Formulation

Based on the above RIS partitioning design, the total number of variables for passive beamforming optimization is reduced from N to $4S$, including the RIS partitioning vector $\mathbf{t} = [t_1, \dots, t_S]^T \in \mathbb{R}^S$, the phase gradients $\mathbf{G} = [\mathbf{g}_1, \dots, \mathbf{g}_S] \in \mathbb{C}^{2 \times S}$, and the common phase shifts $\boldsymbol{\psi} = [\psi_1, \dots, \psi_S]^T \in \mathbb{C}^S$. We aim to maximize the RIS-aided MIMO channel capacity by jointly optimizing the transmit covariance matrix \mathbf{Q} and the RIS reflection matrix Θ , subject to the total power constraint at the Tx and the constraints introduced by RIS partitioning. This problem is formulated as

$$\begin{aligned}
 \text{(P1): } \quad & \max_{\mathbf{Q}, \Theta(\mathbf{t}, \mathbf{G}, \boldsymbol{\psi})} \log \det \left(\mathbf{I}_{M_r} + \frac{1}{\sigma^2} \mathbf{H}_{\text{eff}} \mathbf{Q} \mathbf{H}_{\text{eff}}^H \right) \\
 \text{s. t. } \quad & \text{C1: } \text{tr}(\mathbf{Q}) \leq P, \quad \text{C2: } \mathbf{Q} \succeq \mathbf{0}, \\
 & \text{C3: } \sum_{s \in \mathcal{S}} t_s = 1, \quad \text{C4: } t_s N_y \in \mathbb{Z}_+, \forall s \in \mathcal{S}, \\
 & \text{C5: } \mathbf{g}_s \in \mathcal{F}, \forall s \in \mathcal{S}, \quad \text{C6: } \psi_s \in [0, 2\pi), \forall s \in \mathcal{S}.
 \end{aligned}$$

The difficulty for solving (P1) is twofold. Firstly, due to C4, the optimization w.r.t. \mathbf{t} is an *integer programming* problem that is known to be NP-complete [26]. Secondly, C5 restricts the phase gradients to discrete values, which makes the problem even harder. As such, the RIS partitioning based system design seems to complicate the beamforming design problem. However, we next show that (P1) has a rather simple expression in the asymptotic regime, and the asymptotically optimal solution can serve as a guideline for the finite-size system design.

III. ASYMPTOTIC EXPRESSION OF (P1)

RIS-assisted MIMO systems in next-generation wireless networks are foreseeable to support a large number of antennas at the Tx and Rx, as well as a very large number of reflecting elements at the RIS. This inspires us to study the formulation of (P1) in the asymptotic regime where M_t , M_r , N_x , and N_y go to infinity, i.e.,

$$M_t, M_r, N_x, N_y \rightarrow \infty. \quad (12)$$

To this end, we rewrite the cascaded channel as

$$\begin{aligned}
\sqrt{\text{PL}^r} \mathbf{H}_2 \Theta \mathbf{H}_1 &= \sqrt{\frac{\text{PL}^r M_r M_t}{L_1 L_2}} N \left(\sum_{v=1}^{L_2} \beta_v \mathbf{a}_{M_r}(\vartheta_v) \mathbf{b}_N^H(\vartheta_v^{\text{el}}, \vartheta_v^{\text{az}}) \right) \Theta \left(\sum_{u=1}^{L_1} \alpha_u \mathbf{b}_N(\phi_u^{\text{el}}, \phi_u^{\text{az}}) \mathbf{a}_{M_t}^H(\phi_u) \right) \\
&= \sqrt{\frac{\text{PL}^r M_r M_t}{L_1 L_2}} N \sum_{u=1}^{L_1} \sum_{v=1}^{L_2} \alpha_u \beta_v \mathbf{a}_{M_r}(\vartheta_v) \underbrace{\mathbf{b}_N^H(\vartheta_v^{\text{el}}, \vartheta_v^{\text{az}}) \Theta \mathbf{b}_N(\phi_u^{\text{el}}, \phi_u^{\text{az}})}_{d_{u,v}} \mathbf{a}_{M_t}^H(\phi_u) \\
&= \sqrt{\frac{\text{PL}^r M_r M_t}{L_1 L_2}} N \sum_{u=1}^{L_1} \sum_{v=1}^{L_2} \alpha_u \beta_v d_{u,v} \mathbf{a}_{M_r}(\vartheta_v) \mathbf{a}_{M_t}^H(\phi_u), \tag{13}
\end{aligned}$$

where

$$d_{u,v} = \frac{1}{N} \sum_{n_x=1}^{N_x} \sum_{n_y=1}^{N_y} e^{j\theta_n} e^{-jk((n_x-1)\zeta_{x,u,v} + (n_y-1)\zeta_{y,u,v})} \tag{14}$$

is referred to as the *normalized passive beamforming gain* associated with the u -th path from the Tx to the RIS and the v -th path from the RIS to the Rx, with $k = \frac{2\pi d}{\lambda}$ and $n = n_x + (n_y - 1)N_x$. From (13), we observe that the power gain of the (u, v) -th Tx-RIS-Rx path is determined not only by the path gains of the individual Tx-RIS and RIS-Rx channels, i.e., α_u and β_v , but also by the normalized passive beamforming gain $d_{u,v}$ that can be adjusted by controlling the phase shifts of the reflecting elements. For notation simplicity, we define $\eta_{x,s,u,v} \triangleq g_{x,s} - \zeta_{x,u,v}$ and $\eta_{y,s,u,v} \triangleq g_{y,s} - \zeta_{y,u,v}$. Substituting (11) into (14) yields

$$\begin{aligned}
d_{u,v} &= \frac{1}{N} \sum_{s \in \mathcal{S}} e^{j\psi_s} \left(\sum_{n_x=1}^{N_x} e^{jk(n_x-1)\eta_{x,s,u,v}} \sum_{n_y=N_{y,s-1}^{\text{tot}}+1}^{N_{y,s}^{\text{tot}}} e^{jk(n_y-1)\eta_{y,s,u,v}} \right) \\
&= \sum_{s \in \mathcal{S}} e^{j\psi_s} \left(e^{j\frac{k}{2}(N_x-1)\eta_{x,s,u,v}} \frac{\text{sinc}\left(\frac{k}{2}N_x\eta_{x,s,u,v}\right)}{\text{sinc}\left(\frac{k}{2}\eta_{x,s,u,v}\right)} \right) \left(e^{j\frac{k}{2}(N_{y,s}^{\text{tot}}+N_{y,s-1}^{\text{tot}}-1)\eta_{y,s,u,v}} t_s \frac{\text{sinc}\left(\frac{k}{2}t_s N_y \eta_{y,s,u,v}\right)}{\text{sinc}\left(\frac{k}{2}\eta_{y,s,u,v}\right)} \right) \\
&= \sum_{s \in \mathcal{S}} e^{j\tilde{\psi}_s} t_s \frac{\text{sinc}\left(\frac{k}{2}N_x\eta_{x,s,u,v}\right) \text{sinc}\left(\frac{k}{2}t_s N_y \eta_{y,s,u,v}\right)}{\text{sinc}\left(\frac{k}{2}\eta_{x,s,u,v}\right) \text{sinc}\left(\frac{k}{2}\eta_{y,s,u,v}\right)}, \tag{15}
\end{aligned}$$

where

$$\tilde{\psi}_s = \psi_s + \frac{k}{2}(N_x - 1)\eta_{x,s,u,v} + \frac{k}{2}(N_{y,s}^{\text{tot}} + N_{y,s-1}^{\text{tot}} - 1)\eta_{y,s,u,v}, \tag{16}$$

with $N_{y,s}^{\text{tot}} \triangleq \sum_{i=1}^s N_{y,i}$ denoting the total number of columns of the first s sub-surface(s), $s \in \mathcal{S}$, and $N_{y,0}^{\text{tot}} \triangleq 0$. Eq. (15) represents $d_{u,v}$ as the summation of the passive beamforming gain brought by each sub-surface. The expression in (15) is still complicated due to the involvement of sinc functions.

We now introduce the asymptotic condition $N_x, N_y \rightarrow \infty$ to simplify $d_{u,v}$ as

$$\lim_{N_x, N_y \rightarrow \infty} d_{u,v} = \sum_{s \in \mathcal{S}} \mathbb{1}\{\eta_{x,s,u,v}, \eta_{y,s,u,v}\} e^{j\tilde{\psi}_s t_s}, \quad (17)$$

where the indicator function $\mathbb{1}\{a, b\}$ is defined as

$$\mathbb{1}\{a, b\} = \begin{cases} 1, & a = b = 0, \\ 0, & \text{otherwise.} \end{cases} \quad (18)$$

The condition $\eta_{x,s,u,v} = \eta_{y,s,u,v} = 0$ means that the phase gradient \mathbf{g}_s of sub-surface s is designed to reflect the signals from the AoA $(\phi_u^{\text{el}}, \phi_u^{\text{az}})$ to the AoD $(\vartheta_v^{\text{el}}, \vartheta_v^{\text{az}})$, or equivalently, to align the u -th path of the Tx-RIS channel with the v -th path of the RIS-Rx channel. Eq. (17) shows that when the RIS is infinitely large, only the sub-surfaces that exactly align $(\phi_u^{\text{el}}, \phi_u^{\text{az}})$ with $(\vartheta_v^{\text{el}}, \vartheta_v^{\text{az}})$ contribute to the passive beamforming gain $d_{u,v}$ of the (u, v) -th Tx-RIS-Rx path.

In the following, we show that in the considered asymptotic regime, restricting each Tx-RIS (or RIS-Rx) path to be served by at most one sub-surface does not lose the optimality of (P1).

- With $M_t, M_r \rightarrow \infty$, both the Tx and the Rx have infinite spatial resolution to create orthogonal sub-channels for different paths. If there exists more than one sub-surface serving the same Tx-RIS-Rx path, we can always adjust the corresponding common phase shifts to maximize the received power through this path and thus improve the achievable rate. This adjustment is equivalent to merging the involved sub-surfaces into a single sub-surface.
- If there exists two sub-surfaces serving a common Tx-RIS (or RIS-Rx) path but different RIS-Rx (or Tx-RIS) paths, the cascaded channel constructed by the two sub-surfaces is rank-one and thus cannot support multiplexing. Letting both the two sub-surfaces align with the stronger RIS-Rx (or Tx-RIS) path results in a higher received power, and hence achieves a higher data rate. Thus, the two sub-surfaces can be merged into one sub-surface.

Therefore, for given (u, v) , there is at most one term in the summation of (17) being non-zero. Moreover, the maximum number of sub-surfaces required to achieve the asymptotically optimal solution is $\min\{L_1, L_2\}$, i.e., $S \leq \min\{L_1, L_2\}$.

Remark 2. For the case of $S = \min\{L_1, L_2\}$, the asymptotically optimal solution are achieved with arbitrary common phase shifts of the sub-surfaces, since the served Tx-RIS-Rx path pairs are asymptotically orthogonal to each other. Consider the case that the RIS is partitioned into more than $\min\{L_1, L_2\}$ sub-surfaces, i.e., $S > \min\{L_1, L_2\}$. This case can also achieve the asymptotically optimal solution when some of the sub-surfaces serving the same Tx-RIS-Rx

path pair with properly adjusted common phase shifts. Although achieving the same asymptotic performance, the latter case results in a larger optimization space and the adjustment of common phase shifts incurs additional computational cost. Thus, the case of $S = \min\{L_1, L_2\}$ achieves a better performance-complexity tradeoff than the case of $S > \min\{L_1, L_2\}$.

Based on the above, the optimization of the phase gradients \mathbf{G} reduces to the *tripartite matching* of the Tx-RIS paths, the sub-surfaces, and the RIS-Rx paths. From (17), the passive beamforming gain of a Tx-RIS-Rx path is determined by the partition ratio t_s and the common phase shift ψ_s of the serving sub-surface s , and is irrelevant to the specific position of sub-surface s on the RIS. This implies that the specific position of a sub-surface on the RIS does not affect the performance in the asymptotic regime. Thus, the tripartite matching problem reduces to the *bipartite matching* between the Tx-RIS paths and the RIS-Rx paths. As such, we define a path pairing matrix $\mathbf{B} \in \mathbb{C}^{L_1 \times L_2}$ with $b_{u,v}$ being the (u, v) -th entry of \mathbf{B} . When there exists a sub-surface to align the u -th Tx-RIS path to the v -th RIS-Rx path, the corresponding entry of \mathbf{B} is given by $b_{u,v} = 1$; otherwise $b_{u,v} = 0$. The path pairing constraint is expressed as

$$\text{C7: } \begin{cases} \sum_{u=1}^{L_1} b_{u,v} \leq 1, \forall v, \\ \sum_{v=1}^{L_2} b_{u,v} \leq 1, \forall u, \\ b_{u,v} \in \{0, 1\}, \forall u, v, \\ \sum_{u=1}^{L_1} \sum_{v=1}^{L_2} b_{u,v} = S. \end{cases}$$

The effective channel \mathbf{H}_{eff} can be rewritten as

$$\mathbf{H}_{\text{eff}} = \sqrt{\frac{\text{PL}^r M_r M_t}{L_1 L_2}} N \mathbf{A}_{M_r}(\boldsymbol{\vartheta}) \boldsymbol{\Sigma} \mathbf{A}_{M_t}^H(\boldsymbol{\phi}) + \sqrt{\frac{\text{PL}^d M_r M_t}{L_3}} \mathbf{A}_{M_r}(\boldsymbol{\varphi}) \text{diag}(\boldsymbol{\gamma}) \mathbf{A}_{M_t}^H(\boldsymbol{\omega}), \quad (19)$$

where $\mathbf{A}_{M_r}(\boldsymbol{\vartheta}) \triangleq [\mathbf{a}_{M_r}(\vartheta_1), \dots, \mathbf{a}_{M_r}(\vartheta_{L_2})]$ collects the L_2 arrival steering vectors at the Rx. Similar definitions are applied to $\mathbf{A}_{M_t}(\boldsymbol{\phi})$, $\mathbf{A}_{M_r}(\boldsymbol{\varphi})$, and $\mathbf{A}_{M_t}(\boldsymbol{\omega})$, i.e., $\mathbf{A}_{M_t}(\boldsymbol{\phi}) \triangleq [\mathbf{a}_{M_t}(\phi_1), \dots, \mathbf{a}_{M_t}(\phi_{L_1})]$, $\mathbf{A}_{M_r}(\boldsymbol{\varphi}) \triangleq [\mathbf{a}_{M_r}(\varphi_1), \dots, \mathbf{a}_{M_r}(\varphi_{L_3})]$, and $\mathbf{A}_{M_t}(\boldsymbol{\omega}) \triangleq [\mathbf{a}_{M_t}(\omega_1), \dots, \mathbf{a}_{M_t}(\omega_{L_3})]$. The (v, u) -th entry of $\boldsymbol{\Sigma} \in \mathbb{C}^{L_2 \times L_1}$ is given by $\sigma_{v,u} = \alpha_u \beta_v d_{u,v}$. We notice that $\boldsymbol{\Sigma}$ has S non-zero entries in total, with at most one non-zero entry in each row/column. Hence, we delete the steering vectors in $\mathbf{A}_{M_r}(\boldsymbol{\vartheta})$ and $\mathbf{A}_{M_t}(\boldsymbol{\phi})$ corresponding to the paths that are not served by any sub-surfaces, and rearrange the order of the remaining ones such that $\boldsymbol{\Sigma}$ becomes a diagonal matrix $\tilde{\boldsymbol{\Sigma}}$. Then, the first term of (19) can be equivalently expressed as $\sqrt{\frac{\text{PL}^r M_r M_t}{L_1 L_2}} N \tilde{\mathbf{A}}_{M_r}(\boldsymbol{\vartheta}) \tilde{\boldsymbol{\Sigma}} \tilde{\mathbf{A}}_{M_t}^H(\boldsymbol{\phi})$,

where $\tilde{\mathbf{A}}_{M_r}(\boldsymbol{\vartheta})$ and $\tilde{\mathbf{A}}_{M_t}(\boldsymbol{\phi})$ are respectively the rearranged forms of $\mathbf{A}_{M_r}(\boldsymbol{\vartheta})$ and $\mathbf{A}_{M_t}(\boldsymbol{\phi})$. Define $\mathbf{A}_{M_r} \triangleq [\tilde{\mathbf{A}}_{M_r}(\boldsymbol{\vartheta}), \mathbf{A}_{M_r}(\boldsymbol{\varphi})]$ and $\mathbf{A}_{M_t} \triangleq [\tilde{\mathbf{A}}_{M_t}(\boldsymbol{\phi}), \mathbf{A}_{M_t}(\boldsymbol{\omega})]$, we recast (19) compactly as

$$\mathbf{H}_{\text{eff}} = \mathbf{A}_{M_r} \boldsymbol{\Sigma}_{\text{eff}} \mathbf{A}_{M_t}^H, \quad (20)$$

where

$$\boldsymbol{\Sigma}_{\text{eff}} = \begin{bmatrix} \sqrt{\frac{\text{PL}^r M_r M_t}{L_1 L_2}} N \tilde{\boldsymbol{\Sigma}} & \mathbf{0} \\ \mathbf{0} & \sqrt{\frac{\text{PL}^d M_r M_t}{L_3}} \text{diag}(\boldsymbol{\gamma}) \end{bmatrix}. \quad (21)$$

When $M_t, M_r \rightarrow \infty$, we can readily show that the array response vectors at the Tx and the Rx are asymptotically orthogonal, i.e., $\mathbf{A}_{M_t}^H \mathbf{A}_{M_t} \rightarrow \mathbf{I}$ and $\mathbf{A}_{M_r}^H \mathbf{A}_{M_r} \rightarrow \mathbf{I}$. Therefore, (20) can be approximated as the truncated singular value decomposition (SVD) of \mathbf{H}_{eff} .

With the above asymptotic SVD representation of \mathbf{H}_{eff} , the optimal transmit covariance matrix \mathbf{Q} of (P1) is given by the *eigenmode transmission* [27]:

$$\mathbf{Q}^* = \mathbf{A}_{M_t} \text{diag}\{\mathbf{p}\} \mathbf{A}_{M_t}^H, \quad (22)$$

where $\mathbf{p} = [(\mathbf{p}^r)^T, (\mathbf{p}^d)^T]^T = [p_1^r, \dots, p_S^r, p_1^d, \dots, p_{L_3}^d]^T$ with p_s^r being the the transmit power allocated to the s -th Tx-RIS-Rx path, and p_i^d being the transmit power allocated to the i -th Tx-Rx path, respectively. Substituting \mathbf{Q}^* into the objective function of (P1), we obtain

$$C(\mathbf{p}, \mathbf{t}, \mathbf{B}) \triangleq \sum_{s \in \mathcal{S}} \log(1 + m_s^r p_s^r t_s^2) + \sum_{i \in \mathcal{L}_3} \log(1 + m_i^d p_i^d), \quad (23)$$

where $m_s^r \triangleq \text{PL}^r \frac{M_t M_r N^2 |\alpha_{u_s} \beta_{v_s}|^2}{L_1 L_2 \sigma^2}$ with u_s and v_s being the indices of the Tx-RIS and RIS-Rx paths served by the sub-surface s , respectively, $m_i^d \triangleq \text{PL}^d \frac{M_t M_r |\gamma_i|^2}{L_3 \sigma^2}$, and $\mathcal{L}_3 \triangleq \{1, \dots, L_3\}$. Note that the coefficients m_s^r and m_i^d are unbounded if $M_t, M_r, N_x, N_y \rightarrow \infty$. In practice, the values of m_s^r and m_i^d are relatively small since PL^r and PL^d are typically in the order of $10^{-12} \sim 10^{-16}$ and $10^{-6} \sim 10^{-8}$, respectively [18], [28], while M_t and M_r are in the order of hundreds and N is in the order of thousands. Thus, we keep m_s^r and m_i^d as finite-valued parameters in (23).

Based on the above, (P1) has the following asymptotic form:

$$\begin{aligned} \text{(P2): } & \max_{\mathbf{p}, \mathbf{t}, \mathbf{B}} C(\mathbf{p}, \mathbf{t}, \mathbf{B}) \\ \text{s. t. } & \text{C8: } p_s^r \geq 0, \forall s \in \mathcal{S}, \quad \text{C9: } p_i^d \geq 0, \forall i \in \mathcal{L}_3, \\ & \text{C10: } \sum_{s \in \mathcal{S}} p_s^r + \sum_{i \in \mathcal{L}_3} p_i^d = P, \\ & \text{C11: } t_s \geq 0, \forall s \in \mathcal{S}, \quad \text{C3, C7.} \end{aligned}$$

(P2) is a mixed-integer program, and the objective function is non-convex over the RIS partitioning vector \mathbf{t} . In the next section, we will discuss how to find the optimal solution of \mathbf{p} , \mathbf{t} , and \mathbf{B} to (P2).

IV. OPTIMAL SOLUTION TO (P2)

In this section, we first study the problem of optimizing the power allocation \mathbf{p} and the RIS partitioning \mathbf{t} for any fixed path pairing matrix \mathbf{B} :

$$\begin{aligned} \text{(P3): } \quad & \max_{\mathbf{p}, \mathbf{t}} \quad C(\mathbf{p}, \mathbf{t}) \\ & \text{s. t.} \quad \text{C8, C9, C10, C11, C3,} \end{aligned}$$

where $C(\mathbf{p}, \mathbf{t})$ is an abbreviation of $C(\mathbf{p}, \mathbf{t}, \mathbf{B})$ for fixed \mathbf{B} . Then, we derive the optimal \mathbf{B} in Section IV-D.

A. KKT Conditions of (P3)

The Lagrangian function of (P3) is expressed as

$$\begin{aligned} \mathcal{L}(\mathbf{p}, \mathbf{t}, \boldsymbol{\lambda}, \boldsymbol{\mu}, v, w) = & - \sum_{s \in \mathcal{S}} \log(1 + m_s^r p_s^r t_s^2) - \sum_{i \in \mathcal{L}_3} \log(1 + m_i^d p_i^d) - \sum_{s \in \mathcal{S}} \lambda_s^r p_s^r - \sum_{i \in \mathcal{L}_3} \lambda_i^d p_i^d \\ & + v \left(\sum_{s \in \mathcal{S}} p_s^r + \sum_{i \in \mathcal{L}_3} p_i^d - P \right) - \sum_{s \in \mathcal{S}} \mu_s t_s + w \left(\sum_{s \in \mathcal{S}} t_s - 1 \right), \end{aligned} \quad (24)$$

where $\boldsymbol{\lambda}^r = [\lambda_1^r, \dots, \lambda_S^r]^T$, $\boldsymbol{\lambda}^d = [\lambda_1^d, \dots, \lambda_{L_3}^d]^T$, $\boldsymbol{\mu} = [\mu_1, \dots, \mu_S]^T$, v , and w are the dual variables associated with constraints C8, C9, C11, C10, and C3, respectively, and $\boldsymbol{\lambda} = [(\boldsymbol{\lambda}^r)^T, (\boldsymbol{\lambda}^d)^T]^T$. The stationarity conditions are obtained by setting the first-order derivative of $\mathcal{L}(\mathbf{p}, \mathbf{t}, \boldsymbol{\lambda}, \boldsymbol{\mu}, v, w)$ w.r.t. \mathbf{p} and \mathbf{t} to zero, i.e.,

$$\begin{cases} -\frac{m_s^r t_s^2}{1 + m_s^r p_s^r t_s^2} - \lambda_s^r + v = 0, \forall s \in \mathcal{S}, \end{cases} \quad (25a)$$

$$\begin{cases} -\frac{m_i^d}{1 + m_i^d p_i^d} - \lambda_i^d + v = 0, \forall i \in \mathcal{L}_3, \end{cases} \quad (25b)$$

$$\begin{cases} -\frac{2m_s^r p_s^r t_s}{1 + m_s^r p_s^r t_s^2} - \mu_s + w = 0, \forall s \in \mathcal{S}. \end{cases} \quad (25c)$$

The dual feasibility and complementary slackness conditions are given by

$$\begin{cases} \lambda_s^r \geq 0, \forall s \in \mathcal{S}, \quad \lambda_i^d \geq 0, \forall i \in \mathcal{L}_3, \end{cases} \quad (26a)$$

$$\begin{cases} \lambda_s^r p_s^r = 0, \forall s \in \mathcal{S}, \quad \lambda_i^d p_i^d = 0, \forall i \in \mathcal{L}_3, \end{cases} \quad (26b)$$

$$\begin{cases} \mu_s \geq 0, \forall s \in \mathcal{S}, \end{cases} \quad (26c)$$

$$\begin{cases} \mu_s t_s = 0, \forall s \in \mathcal{S}. \end{cases} \quad (26d)$$

The KKT solutions can be calculated via solving the conditions in (25a)-(25c) and (26a)-(26d), together with the primal feasibility given in the constraints of (P3). As the KKT conditions are the first-order necessary condition for a solution to be optimal, we have the following properties on the optimal power and RIS partitioning strategy.

Lemma 1. *The optimal p_s^r and the optimal t_s to (P3) satisfy the following equation:*

$$t_s = \frac{2v}{w} p_s^r = \frac{1}{P^r} p_s^r, \forall s \in \mathcal{S}, \quad (27)$$

where $P^r = \sum_{i \in \mathcal{S}} p_i^r$ denotes the total power allocated to the cascaded channel.

Proof: We first consider the case of $\{t_s > 0, p_s^r > 0\}$. Combining (25a) and (25c) yields

$$t_s = \frac{2(\lambda_s^r - v)}{\mu_s - w} p_s^r. \quad (28)$$

From the complementary slackness conditions, we have $\lambda_s^r = \mu_s = 0$. Then, summing up (28) for all $s \in \mathcal{S}$, we get $\frac{2v}{w} = \frac{1}{P^r}$, and thus (27) is obtained. Second, (27) holds trivially if $p_s^r = t_s = 0$. What remains is to consider the cases of $\{t_s = 0, p_s^r \neq 0\}$ and $\{t_s \neq 0, p_s^r = 0\}$. These cases are impossible for an optimal pair of $\{t_s, p_s^r\}$ since they cause a waste of either power or reflecting resource. This completes the proof. ■

Lemma 2. *Suppose $m_1^r \geq m_2^r \geq \dots \geq m_S^r$. Then, the entries of the optimal RIS partitioning \mathbf{t} and the optimal power allocation \mathbf{p}^r are both arranged in the descending order, i.e., $t_1 \geq t_2 \geq \dots \geq t_S$ and $p_1^r \geq p_2^r \geq \dots \geq p_S^r$.*

Proof: Suppose without loss of generality that $p_i^r < p_j^r$ for some $j > i$, where $i, j \in \mathcal{S}$. From Lemma 1, we have $t_i < t_j$. For the case of $m_i^r = m_j^r$, $p_i^r < p_j^r$ and $t_i < t_j$ are obviously not the optimal solution. For the case of $m_i^r > m_j^r$, denote the optimal power allocation and RIS partitioning as \mathbf{p} and \mathbf{t} , respectively. Let $\hat{\mathbf{p}} = [p_1^r, \dots, p_{i-1}^r, p_j^r, p_{i+1}^r, \dots, p_{j-1}^r, p_i^r, p_{j+1}^r, \dots, p_S^r, p_1^d, \dots, p_{L_3}^d]^T$ denote a modified transmit power vector, where the only difference between the optimal \mathbf{p} lies in the exchanged ordering of p_i^r and p_j^r . Similarly, we construct a modified RIS partitioning strategy as $\hat{\mathbf{t}} = [t_1, \dots, t_{i-1}, t_j, t_{i+1}, \dots, t_{j-1}, t_i, t_{j+1}, \dots, t_S]^T$. The difference between $C(\hat{\mathbf{p}}, \hat{\mathbf{t}})$ and $C(\mathbf{p}, \mathbf{t})$ is given by

$$C(\hat{\mathbf{p}}, \hat{\mathbf{t}}) - C(\mathbf{p}, \mathbf{t}) = \log \left(1 + \frac{(m_i^r - m_j^r) (p_j^r t_j^2 - p_i^r t_i^2)}{(1 + m_i^r p_i^r t_i^2) (1 + m_j^r p_j^r t_j^2)} \right) > 0, \quad (29)$$

which leads to a contradiction. ■

We next establish the optimal solution to (P3) based on Lemmas 1 and 2. To begin with, we consider two sub-problems of (P3) in the following.

B. Optimal Solutions to (P3.1) and (P3.2)

We construct two sub-problems (P3.1) and (P3.2). Specifically, (P3.1) is to optimize \mathbf{p} with fixed \mathbf{t} , i.e.,

$$\begin{aligned} \text{(P3.1): } \max_{\mathbf{p}} \quad & C(\mathbf{p}) \\ \text{s. t.} \quad & \text{C8, C9, C10,} \end{aligned}$$

where $C(\mathbf{p})$ is an abbreviation of $C(\mathbf{p}, \mathbf{t})$ for fixed \mathbf{t} . The KKT conditions of (P3.1) are given by (25a), (25b), (26a), (26b), C8, C9, and C10. The other sub-problem (P3.2) is constructed as

$$\begin{aligned} \text{(P3.2): } \max_{\mathbf{t}} \quad & C(\mathbf{t}) \triangleq \sum_{s \in \mathcal{S}} \log(1 + \tilde{m}_s t_s^2) \\ \text{s. t.} \quad & \text{C11, C3,} \end{aligned}$$

where $\tilde{m}_s \triangleq m_s p_s^r$ and $C(\mathbf{t})$ is given by $C(\mathbf{p}, \mathbf{t})$ with \mathbf{p} fixed and the constant terms omitted. From Lemma 2, we assume without loss of generality that $\{\tilde{m}\}_{s=1}^S$ are arranged in the descending order. The KKT conditions of (P3.2) are given by (25c), (26c), (26d), C11, and C3. Clearly, the KKT conditions of (P3.1) and (P3.2) are two complementary subsets of those of (P3).

1) *Optimal Solution to (P3.1)*: (P3.1) is convex and its optimal solution is readily given by the *water-filling strategy* [27]:

$$p_s^r = \begin{cases} 0, & \lambda_s^r > 0, \\ \frac{1}{v} - \frac{1}{m_s^r t_s^2}, & \lambda_s^r = 0, \end{cases} \quad \text{and} \quad p_i^d = \begin{cases} 0, & \lambda_i^d > 0, \\ \frac{1}{v} - \frac{1}{m_i^d}, & \lambda_i^d = 0. \end{cases} \quad (30)$$

2) *Optimal Solution to (P3.2)*: (P3.2) is non-convex since the objective function is non-concave w.r.t. \mathbf{t} . Here, we obtain the global maximum of (P3.2) by carefully analysing the KKT conditions.

Lemma 3. *The optimal solution to (P3.2) takes the form of*

$$t_s = \begin{cases} 0, & \mu_s > 0, \\ \frac{1}{w} \pm \sqrt{\frac{1}{w^2} - \frac{1}{\tilde{m}_s}}, & \mu_s = 0. \end{cases} \quad (31)$$

Proof: The optimal solution to (P3.2) satisfies the KKT conditions (25c), (26c) and (26d). If $\mu_s > 0$, we obtain $t_s = 0$ from (26d). Otherwise, $\mu_s = 0$ implies $t_s \geq 0$. The discussion of

$\mu_s = 0$ is thus divided into the cases of $t_s > 0$ and $t_s = 0$. If $t_s > 0$, we have $w = \frac{2\tilde{m}_s t_s}{1+\tilde{m}_s t_s^2} > 0$ by (25c), and correspondingly $t_s = \frac{1}{w} \pm \sqrt{\frac{1}{w^2} - \frac{1}{\tilde{m}_s}}$. If $t_s = 0$, we obtain $w = \frac{2\tilde{m}_s t_s}{1+\tilde{m}_s t_s^2} = 0$. However, there always exists a $t_j > 0$ ($j \neq s$) such that $\mu_j = \frac{2\tilde{m}_j t_j}{1+\tilde{m}_j t_j^2} > 0$, which contradicts the complementary slackness condition by noting $\mu_j t_j > 0$. To summarize, the KKT conditions of (P3.2) are satisfied with $t_s = 0$ if $\mu_s > 0$, and with $t_s = \frac{1}{w} \pm \sqrt{\frac{1}{w^2} - \frac{1}{\tilde{m}_s}}$ if $\mu_s = 0$. This completes the proof. \blacksquare

For notation simplicity, we abbreviate the three possible expressions of each t_s in Lemma 3 as $t_s^0 \triangleq 0$, $t_s^+ \triangleq \frac{1}{w} + \sqrt{\frac{1}{w^2} - \frac{1}{\tilde{m}_s}}$, and $t_s^- \triangleq \frac{1}{w} - \sqrt{\frac{1}{w^2} - \frac{1}{\tilde{m}_s}}$. Define $\mathbf{t}^{\{l_1, l_2, \dots, l_S\}} \triangleq [t_1^{l_1}, t_2^{l_2}, \dots, t_S^{l_S}]^T$ as a candidate solution to (P3.2), where $l_1, l_2, \dots, l_S \in \{0, +, -\}$. Note that for given $\{\tilde{m}_s\}_{s=1}^S$, a specific pattern $\mathbf{t}^{\{l_1, l_2, \dots, l_S\}}$ is not necessarily a valid solution to (P3.2). We need to verify the validity of $\mathbf{t}^{\{l_1, l_2, \dots, l_S\}}$ by checking the feasibility of C3. Also, since C3 possibly has more than one solution, each pattern $\mathbf{t}^{\{l_1, l_2, \dots, l_S\}}$ may correspond to multiple solutions.

We now show that there is no need to exhaustively search over all the possible 3^S patterns specified by (31). In fact, the number of valid solutions is very limited, which allows us to readily find the global optimum. We first consider the special case that the RIS is partitioned to two sub-surfaces.

Lemma 4. *For $S = 2$, the optimal solution to (P3.2) occurs only at $[1, 0]^T$ and $\mathbf{t}^{\{+, +\}}$, which is given by*

$$\mathbf{t} = \begin{cases} [1, 0]^T, & 2 + \sqrt{1 - \frac{\tilde{m}_2}{\tilde{m}_1}} \geq \sqrt{\tilde{m}_2}, \\ \arg \max_{\mathbf{t}} \{C([1, 0]^T), C(\mathbf{t}^{\{+, +\}})\}, & 2 + \sqrt{1 - \frac{\tilde{m}_2}{\tilde{m}_1}} < \sqrt{\tilde{m}_2}. \end{cases} \quad (32)$$

Proof: Please refer to Appendix A. \blacksquare

Proposition 1 generalize the results in Lemma 4 to arbitrary S sub-surfaces.

Proposition 1. *For an arbitrary number S of sub-surfaces, the optimal solution to (P3.2) can appear only at $[1, 0, 0, \dots, 0]^T$, $\mathbf{t}^{\{+, +, 0, \dots, 0\}}$, $\mathbf{t}^{\{+, +, +, \dots, 0\}}$, \dots , $\mathbf{t}^{\{+, +, +, \dots, +\}}$, i.e., the optimal solution is given by*

$$\mathbf{t} = \arg \max_{\mathbf{t}} \{C([1, 0, 0, \dots, 0]^T), C(\mathbf{t}^{\{+, +, 0, \dots, 0\}}), C(\mathbf{t}^{\{+, +, +, \dots, 0\}}), \dots, C(\mathbf{t}^{\{+, +, +, \dots, +\}})\}. \quad (33)$$

Proof: Please refer to Appendix B. \blacksquare

To better understand Proposition 1, in Fig. 3, we plot the achievable rate and the corresponding optimal solution over different transmit SNR $\frac{P}{\sigma^2}$. The coefficients of the paired Tx-RIS-Rx paths

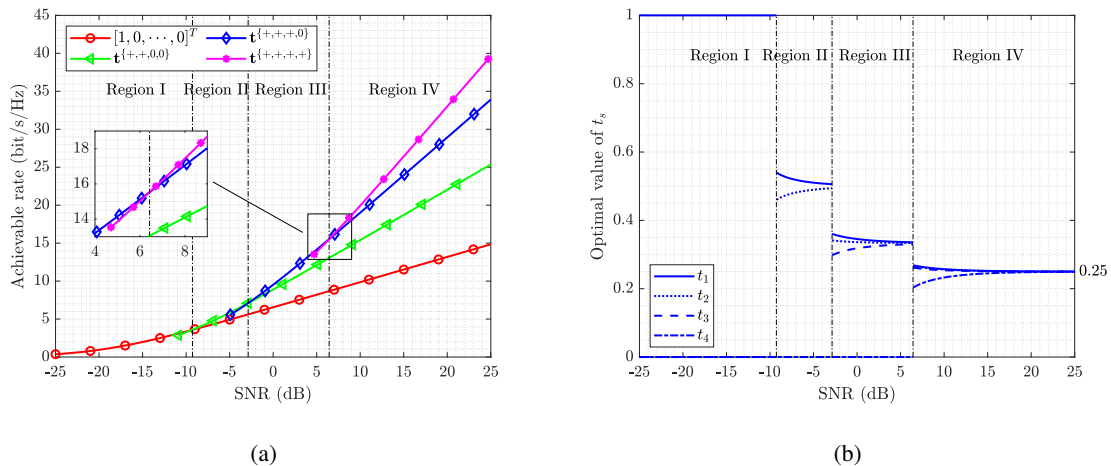


Fig. 3. Numerical illustrations to Proposition 1, where $\min\{L_1, L_2\} = 4$, $m_1 = 93$, $m_2 = 74$, $m_3 = 54$, and $m_4 = 15$.

are set as $m_1 = 93$, $m_2 = 74$, $m_3 = 54$, and $m_4 = 15$. It is assumed that the Tx-Rx direct channel is totally blocked, and the transmit power is equally allocated to the four paired paths. In Regions I, II, III, and IV, the optimal solution is given by activating the first one, two, three, and four paired paths, respectively. In Fig. 3(a), we show that for a given SNR, not every pattern provides a valid solution. It is also observed that multiple solutions (corresponding to multiple patterns) may exist at a given SNR. For instance, the pattern $\mathbf{t}^{(+,+,+,+)}$ appears when the SNR is greater than 4.71 dB, but it becomes the optimal solution only when the SNR exceeds 6.43 dB. This explains why the comparison of multiple patterns is required in (33) to find the optimum. Moreover, we see in Fig. 3(b) that at a relatively low SNR, to maximize the achievable rate, the cascaded channel prefers to concentrate the reflecting resources on a small number of the paired paths, which behaves similar to the water-filling solution. Similarly, when the SNR is high, the cascaded channel prefers to evenly assign the reflecting resources to all the paired paths.

C. Optimal Solution to (P3)

The optimal solution to (P3) is necessarily the optimal solutions to (P3.1) and (P3.2). Besides, Lemma 1 also provides a necessary condition for a solution to be optimal. In the following, we combine these necessary conditions to find the optimal solution to (P3). From Proposition 1, the search over a different number of activated Tx-RIS-Rx paths is required to find the optimum to (P3.2). For this reason, it is necessary to search the optimal solution to (P3) over a different number of activated Tx-RIS-Rx paths and Tx-Rx paths. Denote by \mathcal{S}^a the index set of the activated Tx-RIS-Rx paths, and by \mathcal{I}^a that of the activated Tx-Rx paths. We have $\mathcal{S}^a \in \{\{1\}, \{1, 2\}, \dots, \{1, 2, \dots, S\}\}$ and $\mathcal{I}^a \in \{\{1\}, \{1, 2\}, \dots, \{1, 2, \dots, L_3\}\}$. Given \mathcal{S}^a and

\mathcal{I}^a , combining the aforementioned necessary conditions yields the following system of nonlinear equations:²

$$\left\{ \begin{array}{l} p_s^r = \frac{1}{v} - \frac{1}{m_s^r t_s^2}, s \in \mathcal{S}^a, \\ p_i^d = \frac{1}{v} - \frac{1}{m_i^d}, i \in \mathcal{I}^a, \\ t_s = \frac{1}{w} + \sqrt{\frac{1}{w^2} - \frac{1}{m_s^r p_s^r}}, s \in \mathcal{S}^a, \\ t_s = \frac{2v}{w} p_s^r = \frac{1}{P^r} p_s^r, s \in \mathcal{S}^a, \\ \sum_{s \in \mathcal{S}^a} p_s^r + \sum_{i \in \mathcal{I}^a} p_i^d = P, \\ \sum_{s \in \mathcal{S}^a} t_s = 1. \end{array} \right. \quad \begin{array}{l} (34a) \\ (34b) \\ (34c) \\ (34d) \\ (34e) \\ (34f) \end{array}$$

A key observation of (34) is that, for given v , we immediately obtain the power allocated to each Tx-Rx path from (34b), and the total power allocated to the cascaded channel is thus obtained according to (34e). Moreover, substituting (34d) into (34c) yields the following cubic equation for each s :

$$(p_s^r)^3 - \frac{1}{v} (p_s^r)^2 + \frac{(P^r)^2}{m_s^r} = 0, s \in \mathcal{S}^a, \quad (35)$$

where p_s^r is a valid solution only when $p_s^r \geq \max \left\{ \frac{4v^2 (P^r)^2}{m_s^r}, \frac{1}{2v} \right\}$, by considering that the term in the square root of (34c) is non-negative. Solve (35) for all s and then substitute all the valid solutions into (34e) to verify whether the total power budget is satisfied. If satisfied, we calculate \mathbf{t} and w by (34d) with the obtained \mathbf{p} . In the above process, a 1D exhaustive search over v is required to find all the possible solutions to (34). We provide the implementation details in Algorithm 1. In Line 6, the lower bound of v in the search is given by the maximum of the two arguments, where the first is obtained by plugging (34b) into the inequation $\sum_{s \in \mathcal{S}^a} p_s^r \leq P$, and the second is obtained since $P \geq p_s^r \geq \frac{1}{2v}$. In Line 7, the upper bound of v is given by the minimum of the two arguments, where the first is given by applying $t_s \leq 1$ to (34a), (34b), and (34e), and the second is given by applying $p_i^d \geq 0$ to (34b).

As a low-complexity alternative, the LM method [29], a trust region approach that synthesizes the steepest descent and Gaussian-Newton methods can be adopted to find a stationary point

²For the case of $\mathcal{S}^a = \{1\}$, i.e., $\mathbf{t} = [1, 0, 0, \dots, 0]^T$, the corresponding power allocation can be readily obtained by the water-filling strategy in (30).

Algorithm 1: Proposed 1D Search Algorithm

- 1 **Input:** $\{m_s^r\}_{s=1}^S$, $\{m_i^d\}_{i=1}^{L_3}$, P , searching interval s_{int} , accuracy tolerance ϵ ;
 - 2 **Output:** Optimal solution pair (\mathbf{p}, \mathbf{t}) ;
 - 3 Calculate \mathbf{p} with $\mathbf{t} = [1, 0, 0, \dots, 0]^T$ by (30), and then save (\mathbf{p}, \mathbf{t}) ;
 - 4 **for** $\mathcal{S}^a \in \{\{1, 2\}, \dots, \{1, 2, \dots, S\}\}$ **do**
 - 5 **for** $\mathcal{I}^a \in \{\{1\}, \{1, 2\}, \dots, \{1, 2, \dots, L_3\}\}$ **do**
 - 6 Calculate the search lower bound $b_l = \max \left\{ \frac{|\mathcal{I}^a|}{P + \sum_{i \in \mathcal{I}^a} \frac{1}{m_i^d}}, \frac{1}{2P} \right\}$;
 - 7 Calculate the search upper bound $b_u = \min \left\{ \frac{|\mathcal{I}^a| + |\mathcal{S}^a|}{P + \sum_{i \in \mathcal{I}^a} \frac{1}{m_i^d} + \sum_{s \in \mathcal{S}^a} \frac{1}{m_s^r}}, m_{|\mathcal{I}^a|}^d \right\}$;
 - 8 **for** $v = b_l : s_{\text{int}} : b_u$ **do**
 - 9 Calculate p_i^d by (34b), $\forall i \in \mathcal{I}^a$;
 - 10 Solve the cubic equation (35), $\forall s \in \mathcal{S}^a$;
 - 11 Collect real p_s^r that satisfies $p_s^r \geq \max \left\{ \frac{4v^2(P^r)^2}{m_s^r}, \frac{1}{2v} \right\}$, $\forall s \in \mathcal{S}^a$;
 - 12 Collect all the feasible \mathbf{p} that satisfies $\frac{|\sum_{s \in \mathcal{S}^a} p_s^r + \sum_{i \in \mathcal{I}^a} p_i^d - P|}{P} < \epsilon$;
 - 13 Calculate \mathbf{t} for each feasible \mathbf{p} by (34d), and then save each (\mathbf{p}, \mathbf{t}) ;
 - 14 **end**
 - 15 **end**
 - 16 **end**
 - 17 Return (\mathbf{p}, \mathbf{t}) which yields the maximum achievable rate.
-

of (34). We note that although this alternative method is not guaranteed to reach the optimal solution, simulation results show that its performance is close to the optimal solution found by Algorithm 1.

D. Optimal Path Pairing Strategy

Proposition 2 gives the optimal path pairing matrix \mathbf{B} in closed form.

Proposition 2. Assume without loss of generality that $L_1 \leq L_2$. The optimal path pairing matrix is given by $\mathbf{B} = [\mathbf{I}_{L_1 \times L_1}, \mathbf{0}]$.

Proof: The result is trivial when $L_1 = 1$. When $L_1 = 2$, we only need to compare two different configurations of the pairing matrix, i.e.,

$$\mathbf{B} = \begin{bmatrix} 1 & 0 & 0 & \cdots & 0 \\ 0 & 1 & 0 & \cdots & 0 \end{bmatrix} \text{ and } \check{\mathbf{B}} = \begin{bmatrix} 0 & 1 & 0 & \cdots & 0 \\ 1 & 0 & 0 & \cdots & 0 \end{bmatrix}. \quad (36)$$

Applying \mathbf{B} results in $m_s^r = c|\alpha_s\beta_s|^2$, $s = 1, 2$, and applying $\check{\mathbf{B}}$ results in $m_1^r = c|\alpha_1\beta_2|^2$ and $m_2^r = c|\alpha_2\beta_1|^2$, where $c = \text{PL}^r \frac{M_t M_r N^2}{L_1 L_2 \sigma^2}$. Denote the optimal power and RIS partitioning associated with $\check{\mathbf{B}}$ as $\check{\mathbf{p}} = [\check{p}_1^r, \check{p}_2^r, \check{p}_1^d, \dots, \check{p}_{L_3}^d]^T$ and $\check{\mathbf{t}} = [\check{t}_1, \check{t}_2]^T$, respectively. We have

$$C(\check{\mathbf{p}}, \check{\mathbf{t}}, \mathbf{B}) - C(\check{\mathbf{p}}, \check{\mathbf{t}}, \check{\mathbf{B}}) = \log \left(1 + \frac{c(|\beta_1|^2 - |\beta_2|^2)(|\alpha_1|^2 \check{p}_1^r \check{t}_1^2 - |\alpha_2|^2 \check{p}_2^r \check{t}_2^2)}{(1 + c|\alpha_1\beta_2|^2 \check{p}_1^r \check{t}_1^2)(1 + c|\alpha_2\beta_1|^2 \check{p}_2^r \check{t}_2^2)} \right). \quad (37)$$

Suppose without loss of generality that $|\alpha_1\beta_2| \geq |\alpha_2\beta_1|$, we have $\check{p}_1^r \geq \check{p}_2^r$ and $\check{t}_1 \geq \check{t}_2$ according to Lemma 2. Recall that $|\alpha_1| \geq |\alpha_2|$ and $|\beta_1| \geq |\beta_2|$, we obtain $C(\check{\mathbf{p}}, \check{\mathbf{t}}, \mathbf{B}) - C(\check{\mathbf{p}}, \check{\mathbf{t}}, \check{\mathbf{B}}) \geq 0$ from (37). Moreover, denote by \mathbf{p} and \mathbf{t} the optimal power and RIS partitioning associated with \mathbf{B} , respectively. We have $C(\mathbf{p}, \mathbf{t}, \mathbf{B}) \geq C(\check{\mathbf{p}}, \check{\mathbf{t}}, \mathbf{B}) \geq C(\check{\mathbf{p}}, \check{\mathbf{t}}, \check{\mathbf{B}})$, which completes the proof of the case $L_1 = 2$.

When $L_1 > 2$, suppose that the path pairing matrix is not chosen as in Proposition 2. Then, there always exist two Tx-RIS-Rx path pairs with the corresponding path pairing submatrix given by $\check{\mathbf{B}}$ in (36). By following the argument for the case of $L_1 = 2$, we can replace the submatrix to \mathbf{B} in (36) which do not decrease the achievable rate. Finally, we arrive at the path pairing matrix given in Proposition 2. This concludes the proof. \blacksquare

Since $\{\alpha_\ell\}_{\ell=1}^{L_1}$ and $\{\beta_\ell\}_{\ell=1}^{L_2}$ are both arranged in the descending order of their magnitudes, Proposition 2 shows that the Tx-RIS and RIS-Rx paths are paired in the same order based on their respective path gains. As a final remark, we note that the optimal \mathbf{B} of (P2) can be obtained by Proposition 2 regardless of the values of \mathbf{t} and \mathbf{p} . Then, the optimal \mathbf{t} and \mathbf{p} of (P2) can be calculated by solving (34).

E. Algorithm Design in Finite-Size Systems

We now discuss how to apply the optimization result of (P2) to the finite-size system design. Firstly, $t_s N_y$ may be fractional, and hence is not a feasible solution to (P1). We apply the rounding technique to transform each $t_s N_y$ into an integer. Secondly, the optimization of common phase shifts ψ is not considered in (P2), as an arbitrary value of ψ in the feasible region is asymptotically optimal. However, a different value of ψ results in a different achievable rate in (P1) for a finite-size system. The problem of optimizing ψ can be solved by existing techniques, e.g., the WMMSE method [30]. Different from the work [11] that utilizing the WMMSE method to handle the high-dimensional RIS reflection coefficients directly, we only need to solve ψ in S dimensions with much lower computational complexity. We also note that optimizing ψ becomes

TABLE I
DEFAULT VALUES OF SIMULATION PARAMETERS

Parameter	Value	Parameter	Value
Number of Tx antennas	$M_t = 32$	Transmission bandwidth	$B = 251.1886$ MHz
Number of Rx antennas	$M_r = 32$	Noise power	$\sigma^2 = -90$ dBm
Number of reflecting elements	$N = 30 \times 90$	Transmit power	$P = 30$ dBm
Antenna/element spacing	$d = \frac{1}{2}$	Path loss for the cascaded channel	$PL^r = \frac{\lambda^2}{64\pi^3 d_1^{2.4} d_2^{2.4}}$
Carrier frequency	$f = 28$ GHz	Path loss for the Tx-Rx channel	$PL^d = \frac{\lambda^2}{16\pi^2 d_3^{2.4}}$

less critical when the system size is relatively large. In fact, setting ψ arbitrarily, e.g., $\psi = \mathbf{0}$, does not cause much performance degradation in the RIS-aided large-scale MIMO system.

V. SIMULATION RESULTS

In this section, we provide numerical results to evaluate the performance of the RIS partitioning based beamforming design. Consider a simulation scenario where the distances from the Tx to the RIS, from the RIS to the Rx, and from the Tx to the Rx are set as $d_1 = 100$ m, $d_2 = 60$ m, and $d_3 = 150$ m, respectively. The channel coefficients are generated according to the channel model described in Section II, which is similar to the 3GPP ray-tracing model [25, Section 7.5]. In particular, the AoAs/AoDs are uniformly distributed in the continuous angle range, i.e., $(0, \frac{1}{2}\pi]$ for the elevation angle and $(0, 2\pi]$ for the azimuth angle. The complex gains $\{\alpha_\ell\}_{\ell=1}^{L_1}$, $\{\beta_\ell\}_{\ell=1}^{L_2}$, and $\{\gamma_\ell\}_{\ell=1}^{L_3}$ are generated from the CSCG distribution with zero mean and unit variance, and then rearranged in the respective descending order in magnitude. The numbers of dominant channel paths are given by $L_1 = 5$, $L_2 = 7$, and $L_3 = 4$. Unless otherwise specified, we adopt the default values of the system parameters provided in Table I. It is worth noting that unlike many existing works assuming that the direct link is completely blocked or very weak [7], [8], [10]–[12], [22], we consider a more typical scenario where the path-loss exponents are equally set to 2.4 for both the cascaded and the direct links. The experiments are carried out on a Windows x64 machine with 2.90 GHz CPU and 16 GB RAM by MATLAB R2021b. All results are obtained by averaging over 1000 independent channel realizations.

In Fig. 4, we compare the performance and complexity of the proposed design with the baseline PB-WMMSE method [11] that solves the following problem in two-layer iterations:

$$\begin{aligned}
 \text{(P4): } \quad & \max_{\mathbf{Q}, \Theta} \log \det \left(\mathbf{I}_{M_r} + \frac{1}{\sigma^2} \mathbf{H}_{\text{eff}} \mathbf{Q} \mathbf{H}_{\text{eff}}^H \right) \\
 \text{s. t. } \quad & \text{C12: } \theta_n \in [0, 2\pi), \forall n \in \mathcal{N}, \quad \text{C1, C2.}
 \end{aligned}$$

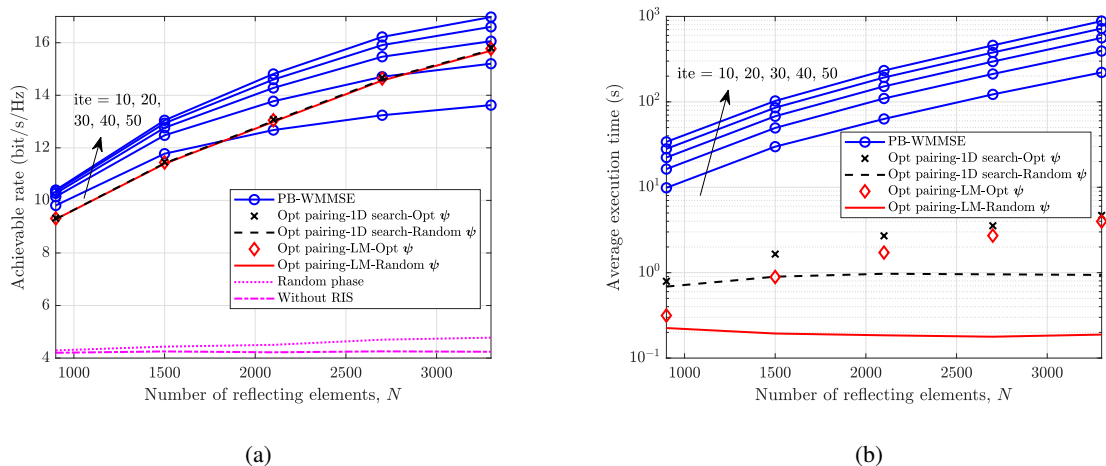


Fig. 4. (a) Achievable rate; (b) average execution time vs. the number of reflecting elements N .

In particular, the outer iteration involves the alternating optimization of \mathbf{Q} and Θ , and the inner iteration involves the WMMSE relaxation. We note that (P4) is a more general form of (P1) by dropping the RIS partitioning constraints. Because of the heavy computation burden of the WMMSE method, we terminate the algorithm after 50 outer iterations, and plot the results when the number of iterations $\text{ite} = 10, 20, 30, 40, 50$. At each outer iteration, the inner iteration stops when the increase of the target function is less than 10^{-4} , or the maximum number of inner iterations (set to 1000) is reached, whichever comes earlier. For the proposed design, we consider four different implementations of the algorithm, where \mathbf{B} is obtained by the optimal path pairing strategy given in Proposition 2, \mathbf{p} and \mathbf{t} are obtained by solving (34) either via the 1D search or via the LM method, and ψ is obtained either by the WMMSE method or by random setting. From Fig. 4(a), we observe that all the four implementations have comparable performance with the PB-WMMSE benchmark. For a moderate number of reflecting elements, e.g., $N = 900$, 30 outer iterations are enough for the PB-WMMSE method to converge, while for $N = 3600$, the performance improvement is still visible after 40 outer iterations. This implies that the convergence speed of the PB-WMMSE benchmark slows down as N becomes large, which further increases the computation burden.

We plot the average execution times of different algorithms against N in Fig. 4(b). The average execution times required by our proposed designs are all less than 5 seconds even when $N = 3600$, while it takes the PB-WMMSE method about 1000 seconds to conduct 50 outer iterations. Such a substantial complexity reduction makes our proposed method a more practical choice for RIS-aided MIMO communications. Remarkably, the proposed LM implementation with random ψ has an extremely low complexity, namely less than 0.23 second to finish execution

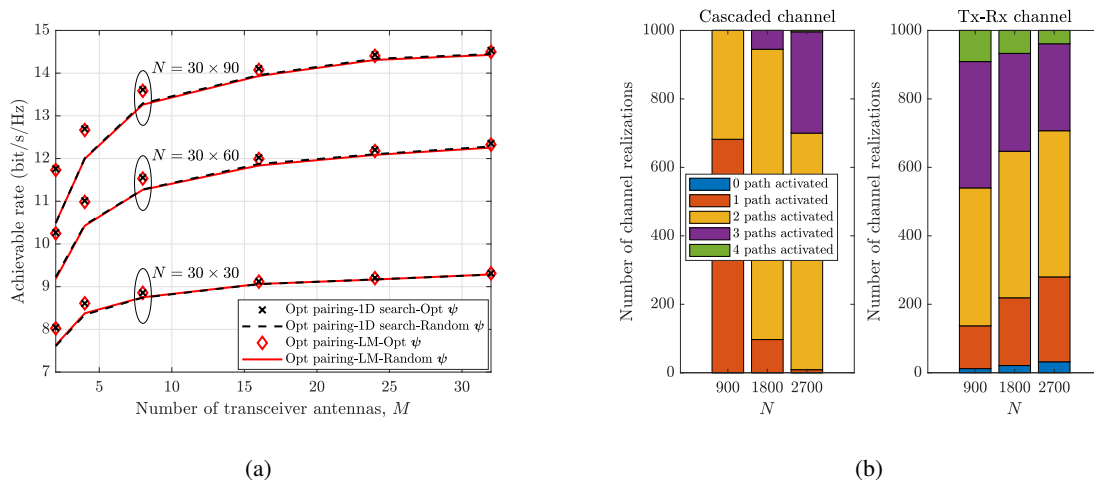


Fig. 5. (a) Achievable rate vs. the number of transceiver antennas M , where we set $M_t = M_r = M$, and the transmit power is set as $P = \frac{P_0}{M_t M_r}$ with $P_0 = 60.1030$ dBm; (b) the occurrence times of different numbers of activated paths in the cascaded channel and the Tx-Rx channel vs. the number of reflecting elements N for the LM method, where $M = 16$.

for all plotted N , and at the same time achieves almost the same performance with the other three proposed implementations in the large-scale MIMO scenario.

Fig. 5(a) plots the achievable rate against the number of transceiver antennas M for different N , where we set $M_t = M_r = M$. The transmit power is normalized by M_t and M_r as $P = \frac{P_0}{M_t M_r}$, where $P_0 = 60.1030$ dBm. It is observed that solving (34) either by the 1D search or by the LM method yields almost the same performance, and the achievable rate differences are mainly brought by different methods for optimizing ψ . In particular, the WMMSE method for optimizing ψ outperforms the random ψ setting when M is relatively small. The reason is that when M is small, the transceiver antenna arrays do not have enough spatial resolution to distinguish signals from different paths. As ψ controls the wavefront phase of the signal transmitted through each paired Tx-RIS-Rx path, it is crucial to choose an appropriate ψ to minimize the inter-path interference caused by limited spatial resolution.

To gain more insights, for the case of $M = 16$ in Fig. 5(a) employing the LM method, we provide in Fig. 5(b) the occurrence times of different numbers of activated Tx-RIS-Rx and Tx-Rx paths in the simulated 1000 independent channel realizations. It is shown that as N increases, the system tends to activate more paths in the cascaded channel for data transmission. For instance, for $N = 900$, the occurrence times for one, two, three and four activated paths in the cascaded channel are 682, 318, 0, and 0, respectively; for $N = 2700$, the corresponding occurrence times become 9, 691, 296, and 4. In contrast, less Tx-Rx paths tend to be activated as N grows. This is because a larger N provides a better link quality for the paths in the cascaded channel.

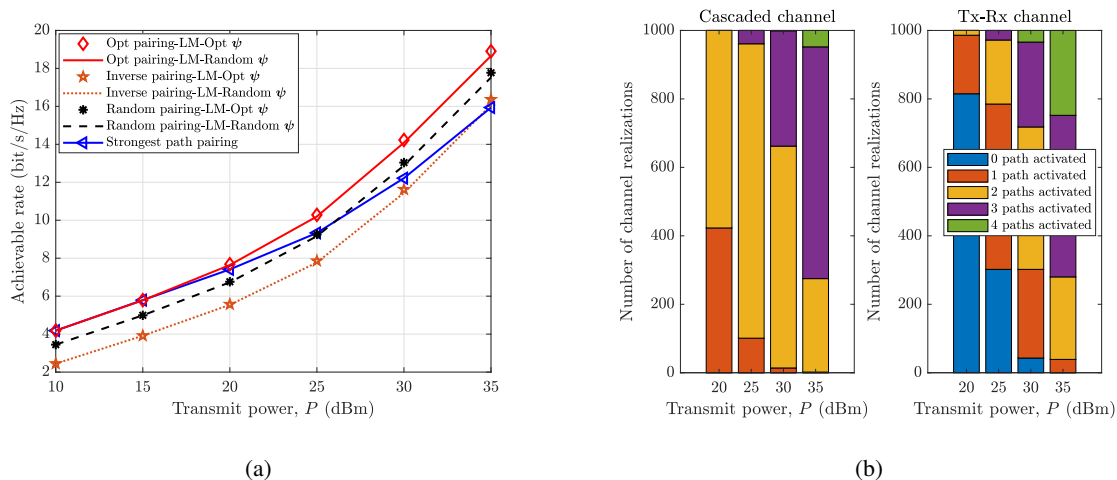


Fig. 6. (a) Achievable rate vs. the transmit power P ; (b) the occurrence times of different numbers of activated paths in the cascaded channel and the Tx-Rx channel vs. the transmit power P for the LM method.

Thus, for a given constant power budget P , more power is dedicated to the transmission through the cascaded channel, and hence more paths in the cascaded channel are activated to support multiplexing.

In Fig. 6(a), we show the achievable rate versus the transmit power P in various path pairing approaches. By comparing the red solid, khaki dotted, and black dashed curves, it is observed that the proposed optimal path pairing strategy has a superior performance compared to the inverse pairing case in which the Tx-RIS and RIS-Rx paths are paired inversely based on their own path gains, and the random pairing case in which the Tx-RIS and RIS-Rx paths are paired randomly. This is in agreement with Proposition 2. In addition, we consider the strongest path pairing strategy, where the RIS is dedicated to only serve the strongest Tx-RIS and RIS-Rx paths. We see that the performance gap between the strongest path pairing strategy and the optimal path pairing strategy is negligible when P is small. This can be explained in Fig. 6(b), which depicts the occurrence times of different numbers of activated paths vs. the transmit power P employing the LM method. In the low SNR regime, i.e., $P = 20$ dBm, the LM method only activate one or two paths in the cascaded channel for data transmission, where the strongest path pairing strategy is close to optimal. However, as the transmit power increases, more paths in the cascaded channel need to be activated, which leads to an increased gap between the optimal pairing strategy with the LM method and the strongest path pairing strategy.

VI. CONCLUSIONS

In this paper, we proposed a RIS-partitioning-based scalable beamforming design for RIS-aided large-scale MIMO systems. We formulated the achievable rate maximization problem by jointly

optimizing active and passive beamforming, where the passive beamforming optimization reduces to the manipulation of the sub-surface sizes, the phase gradients of sub-surfaces, and the common phase shifts of sub-surfaces. We first focused on the asymptotic regime where the numbers of transceiver antennas and RIS elements go to infinity. The asymptotic formulation of the problem yields a clear and simple form, which allows to characterize the fundamental performance-complexity tradeoff of RIS partitioning. Moreover, we developed an efficient algorithm to obtain the asymptotically optimal solution via efficient 1D search. We also presented the LM method to reach a stationary point with an extremely low complexity. Then, we discussed the insights and impacts of the asymptotically optimal solution on finite-size system design. Simulation results demonstrated appealing performance and low complexity of the proposed RIS partitioning design.

APPENDIX A

PROOF OF LEMMA 4

There are $3^S = 9$ possible patterns of the KKT solutions to (P3.2) for $S = 2$. Firstly, we note that the pattern $\mathbf{t}^{\{0,0\}}$ does not exist since $t_1^0 + t_2^0 = 1$ cannot hold in any circumstance. We discuss the optimality of the remaining eight patterns subsequently.

A. $\mathbf{t}^{\{-,0\}}$, $\mathbf{t}^{\{+,0\}}$, $\mathbf{t}^{\{0,-\}}$, and $\mathbf{t}^{\{0,+ \}}$

1) $\mathbf{t}^{\{-,0\}}$ and $\mathbf{t}^{\{+,0\}}$: Substituting the expression of $\mathbf{t}^{\{-,0\}}$ into C3 yields

$$1 - \sqrt{1 - \frac{w^2}{\tilde{m}_1}} = w, \quad (38)$$

where $0 < w \leq \sqrt{\tilde{m}_1}$. It can be readily verified that the above equation has a solution when $0 < \tilde{m}_1 \leq 1$, and the solution is unique due to the monotonicity of (38). Similarly, the pattern $\mathbf{t}^{\{+,0\}}$ exists when $\tilde{m}_1 > 1$ and also corresponds to a unique KKT solution. We remark that $\mathbf{t}^{\{-,0\}}$ and $\mathbf{t}^{\{+,0\}}$ correspond to the same solution $\mathbf{t} = [1, 0]^T$ even though they have different patterns.

2) $\mathbf{t}^{\{0,-\}}$ and $\mathbf{t}^{\{0,+ \}}$: Similarly, the existence conditions of the patterns $\mathbf{t}^{\{0,-\}}$ and $\mathbf{t}^{\{0,+ \}}$ are given as $0 < \tilde{m}_2 \leq 1$ and $\tilde{m}_2 > 1$, respectively. Also, they correspond to the same solution $\mathbf{t} = [0, 1]^T$. However, since $\tilde{m}_2 \leq \tilde{m}_1$, the achievable rate at $\mathbf{t} = [0, 1]^T$ cannot be greater than that at $\mathbf{t} = [1, 0]^T$, i.e., $\log(1 + \tilde{m}_2) \leq \log(1 + \tilde{m}_1)$.

B. $\mathbf{t}^{\{-,+ \}}$, $\mathbf{t}^{\{+,- \}}$, $\mathbf{t}^{\{+,+ \}}$, and $\mathbf{t}^{\{-,- \}}$

1) $\mathbf{t}^{\{-,+ \}}$: Substituting the expression of the pattern $\mathbf{t}^{\{-,+ \}}$ into C3 yields

$$2 - \sqrt{1 - \frac{w^2}{\tilde{m}_1}} + \sqrt{1 - \frac{w^2}{\tilde{m}_2}} = w, \quad (39)$$

where $0 < w \leq \sqrt{\tilde{m}_2}$. It can be readily verified that the above equation has solution when

$$2 - \sqrt{1 - \frac{\tilde{m}_2}{\tilde{m}_1}} < \sqrt{\tilde{m}_2}, \quad (40)$$

and the solution is unique due to the monotonicity of (39). Thus, we use $\mathbf{t}^{\{-,+\}}$ in the following to represent the corresponding KKT solution without causing ambiguity. Next, we prove that $\mathbf{t}^{\{-,+\}}$ is not a globally optimal solution for any \tilde{m}_1 and \tilde{m}_2 , provided that the existence condition in (40) is satisfied. In this regard, we treat (39) as an implicit function of w w.r.t. \tilde{m}_1 and \tilde{m}_2 . The partial derivative $\partial w / \partial \tilde{m}_1$ can be expressed as

$$\frac{\partial w}{\partial \tilde{m}_1} = \frac{w^2}{2\tilde{m}_1 \sqrt{\tilde{m}_1^2 - \tilde{m}_1 w^2}} \left(\frac{w}{\sqrt{\tilde{m}_1^2 - \tilde{m}_1 w^2}} - \frac{w}{\sqrt{\tilde{m}_2^2 - \tilde{m}_2 w^2}} - 1 \right)^{-1}. \quad (41)$$

It can be observed from (41) that $\partial w / \partial \tilde{m}_1 < 0$ since $\frac{w}{\sqrt{\tilde{m}_1^2 - \tilde{m}_1 w^2}} - \frac{w}{\sqrt{\tilde{m}_2^2 - \tilde{m}_2 w^2}} \leq 0$. Then, we have

$$\frac{\partial t_1^-}{\partial \tilde{m}_1} = -\frac{\partial t_2^+}{\partial \tilde{m}_1} = -\frac{\partial t_2^+}{\partial w} \frac{\partial w}{\partial \tilde{m}_1} < 0. \quad (42)$$

where the first step is due to $t_1^- + t_2^+ = 1$, and the second step is from the chain rule. It can be shown that $t_1^- t_2^+$ is monotonically decreasing as the increase of \tilde{m}_1 , since

$$\frac{\partial (t_1^- t_2^+)}{\partial \tilde{m}_1} = t_2^+ \frac{\partial t_1^-}{\partial \tilde{m}_1} + t_1^- \frac{\partial t_2^+}{\partial \tilde{m}_1} = (t_2^+ - t_1^-) \frac{\partial t_1^-}{\partial \tilde{m}_1} < 0. \quad (43)$$

Since $\tilde{m}_1 \geq \tilde{m}_2$, from (43) we obtain $t_1^- t_2^+ \leq t_1^- t_2^+ \Big|_{\tilde{m}_1 = \tilde{m}_2} = \left(\frac{1}{w} - \sqrt{\frac{1}{w^2} - \frac{1}{\tilde{m}_1}} \right) \left(\frac{1}{w} + \sqrt{\frac{1}{w^2} - \frac{1}{\tilde{m}_2}} \right) = \frac{1}{\tilde{m}_2}$. We now show that the achievable rate at $\mathbf{t}^{\{-,+\}}$ cannot be greater than that at $\mathbf{t} = [1, 0]^T$:

$$\begin{aligned} C(\mathbf{t}^{\{-,+\}}) &= \log(1 + \tilde{m}_1 (t_1^-)^2) + \log(1 + \tilde{m}_2 (t_2^+)^2) \\ &\leq \log(1 + \tilde{m}_1 ((t_1^-)^2 + (t_2^+)^2 + \tilde{m}_2 (t_1^- t_2^+)^2)) \\ &= \log(1 + \tilde{m}_1 (1 - 2t_1^- t_2^+ + \tilde{m}_2 (t_1^- t_2^+)^2)) \\ &\leq \log(1 + \tilde{m}_1) = C([1, 0]^T), \end{aligned} \quad (44)$$

where the third step applies the fact that $(t_1^-)^2 + (t_2^+)^2 = (t_1^- + t_2^+)^2 - 2t_1^- t_2^+$, and the fourth step is obtained by taking the maximum of the quadratic function $t_1^- t_2^+ \mapsto 1 - 2t_1^- t_2^+ + \tilde{m}_2 (t_1^- t_2^+)^2$ over $(0, \frac{1}{\tilde{m}_2}]$. This shows that $\mathbf{t}^{\{-,+\}}$ does not yield a global optimum.

2) $\mathbf{t}^{\{+,-\}}$: When the pattern $\mathbf{t}^{\{+,-\}}$ exists, it corresponds to two KKT solutions. The achievable rates at the two KKT solutions can be shown to be no greater than that at $\mathbf{t} = [1, 0]^T$ by following almost the same arguments in discarding $\mathbf{t}^{\{-,+\}}$. We omit the details here.

3) $\mathbf{t}^{\{+,+\}}$: We prove the pattern $\mathbf{t}^{\{+,+\}}$ corresponds to a local maximum as follows. Firstly, the existence condition of $\mathbf{t}^{\{+,+\}}$ is given by

$$2 + \sqrt{1 - \frac{\tilde{m}_2}{\tilde{m}_1}} < \sqrt{\tilde{m}_2}. \quad (45)$$

It is observed that $\tilde{m}_2 > 4$ is a necessary condition for the above inequality to hold. Moreover, if the pattern $\mathbf{t}^{\{+,+\}}$ exists (i.e., the existence condition in (45) is satisfied), the KKT solution employs this pattern is also shown to be unique (for the same reason of the case $\mathbf{t}^{\{-,+\}}$). Thus, we use $\mathbf{t}^{\{+,+\}}$ in the following to represent the corresponding KKT solution without causing ambiguity. Substituting $t_2^+ = 1 - t_1^+$ into the objective function of (P3.2) to eliminate t_2^+ , we recast the problem as

$$\max_{0 \leq t_1^+ \leq 1} C(t_1^+) = \log(1 + \tilde{m}_1(t_1^+)^2) + \log(1 + \tilde{m}_2(1 - t_1^+)^2). \quad (46)$$

The second-order derivative of $C(t_1^+)$ is given by

$$\frac{\partial^2 C}{\partial (t_1^+)^2} = \frac{2\tilde{m}_1(1 - \tilde{m}_1(t_1^+)^2)}{(1 + \tilde{m}_1(t_1^+)^2)^2} + \frac{2\tilde{m}_2(1 - \tilde{m}_2(t_2^+)^2)}{(1 + \tilde{m}_2(t_2^+)^2)^2}. \quad (47)$$

We observe from $t_2^+ = \frac{1}{w} + \sqrt{\frac{1}{w^2} - \frac{1}{\tilde{m}_2}}$ that for any fixed \tilde{m}_2 , t_2^+ decreases with the increase of w . Based on the monotonicity, we have $t_2^+ \geq 1/\sqrt{\tilde{m}_2}$ since $w \leq \sqrt{\tilde{m}_2}$. This shows that the second term of $\partial^2 C / \partial (t_1^+)^2$ in (47) is non-positive. Moreover, considering that $t_1^+ = \frac{1}{w} + \sqrt{\frac{1}{w^2} - \frac{1}{\tilde{m}_1}}$, $t_2^+ = \frac{1}{w} + \sqrt{\frac{1}{w^2} - \frac{1}{\tilde{m}_2}}$, $t_1^+ + t_2^+ = 1$, and $\tilde{m}_1 \geq \tilde{m}_2 > 4$, we have $t_2^+ \leq \frac{1}{2} \leq t_1^+$. Hence, $\tilde{m}_1(t_1^+)^2 > 1$ and the first term of $\partial^2 C / \partial (t_1^+)^2$ is less than zero. We conclude that $\partial^2 C / \partial (t_1^+)^2 < 0$, which implies that $\mathbf{t}^{\{+,+\}}$ corresponds to a local maximum.

4) $\mathbf{t}^{\{-,-\}}$: The pattern $\mathbf{t}^{\{-,-\}}$ corresponds to a local minimum if it exists. The proof is similar to the case of $\mathbf{t}^{\{+,+\}}$ and the details are omitted for brevity.

Based on the discussions above, we conclude that when $S = 2$, the optimal solution to (P3.2) occurs only at $\mathbf{t}^{\{-,0\}}$, $\mathbf{t}^{\{+,0\}}$, and $\mathbf{t}^{\{+,+\}}$, in which the first two patterns correspond to the same solution $\mathbf{t} = [1, 0]^T$. This completes the proof of Lemma 4.

APPENDIX B

PROOF OF PROPOSITION 1

For $S = 2$, Proposition 1 can be readily proven by Lemma 4. Thus, it suffices to consider the case of $S > 2$. We next show that the optimal solution can be obtained by comparing the S solutions given in Proposition 1. Firstly, if $t_i^0 = 0$, we have $t_j^0 = 0$ for all $j > i$ according to Lemma 2. Secondly, we prove by contradiction that the patterns t_i^+ and t_j^- ($i \neq j$) cannot

co-exist in the optimal solution. Suppose that the opposite is true. Then, $[t_i^+, t_j^-]^T$ is necessarily the optimal solution to the following problem:

$$\max_{[t_i, t_j]^T} \log(1 + \tilde{m}_i t_i^2) + \log(1 + \tilde{m}_j t_j^2) \quad (48a)$$

$$\text{s. t. } t_i \geq 0, \quad t_j \geq 0, \quad (48b)$$

$$t_i + t_j = 1 - \sum_{k \in \mathcal{S} \setminus \{i, j\}} t_k. \quad (48c)$$

The only difference between the above problem and the problem considered in Lemma 4 lies in the different RIS partitioning budget in (48c). The discussion in Lemma 4 can be directly applied here to show that the pattern $[t_i^+, t_j^-]^T$ cannot reach the optimum of the problem in (48), which leads to a contradiction. Thirdly, following similar arguments, we can prove that t_i^- and t_j^- ($i \neq j$) cannot co-exist in the optimal solution. Based on the above, we conclude that the optimal solution only occurs at $\mathbf{t}^{\{-,0,0,\dots,0\}}$, $\mathbf{t}^{\{+,0,0,\dots,0\}}$, $\mathbf{t}^{\{+,+,0,\dots,0\}}$, $\mathbf{t}^{\{+,+,+,0,\dots,0\}}$, \dots , and $\mathbf{t}^{\{+,+,+, \dots, +\}}$, where the first two patterns correspond to the same solution $\mathbf{t} = [1, 0, 0, \dots, 0]^T$. Moreover, each pattern corresponds to a unique solution provided that its existence condition is satisfied. This can be shown by plugging the expressions into C3. The proof concludes here.

REFERENCES

- [1] K. B. Letaief, W. Chen, Y. Shi, J. Zhang, and Y.-J. A. Zhang, "The roadmap to 6G: AI empowered wireless networks," *IEEE Commun. Mag.*, vol. 57, no. 8, pp. 84–90, 2019.
- [2] N. Yu, P. Genevet, M. A. Kats, F. Aieta, J.-P. Tetienne, F. Capasso, and Z. Gaburro, "Light propagation with phase discontinuities: generalized laws of reflection and refraction," *Science*, vol. 334, no. 6054, pp. 333–337, 2011.
- [3] T. J. Cui, M. Q. Qi, X. Wan, J. Zhao, and Q. Cheng, "Coding metamaterials, digital metamaterials and programmable metamaterials," *Light, Sci. Appl.*, vol. 3, no. 10, pp. e218–e218, 2014.
- [4] M. Di Renzo, M. Debbah, D.-T. Phan-Huy, A. Zappone, M.-S. Alouini, C. Yuen, V. Sciancalepore, G. C. Alexandropoulos, J. Hoydis, H. Gacanin *et al.*, "Smart radio environments empowered by reconfigurable AI meta-surfaces: An idea whose time has come," *EURASIP J. on Wireless Commun. and Netw.*, vol. 2019, no. 1, pp. 1–20, 2019.
- [5] C. Liaskos, S. Nie, A. Tsioliaridou, A. Pitsillides, S. Ioannidis, and I. Akyildiz, "A new wireless communication paradigm through software-controlled metasurfaces," *IEEE Commun. Mag.*, vol. 56, no. 9, pp. 162–169, 2018.
- [6] X. Yuan, Y.-J. A. Zhang, Y. Shi, W. Yan, and H. Liu, "Reconfigurable-intelligent-surface empowered wireless communications: Challenges and opportunities," *IEEE Wireless Commun.*, vol. 28, no. 2, pp. 136–143, 2021.
- [7] Q. Wu and R. Zhang, "Intelligent reflecting surface enhanced wireless network via joint active and passive beamforming," *IEEE Trans. Wireless Commun.*, vol. 18, no. 11, pp. 5394–5409, 2019.
- [8] H. Guo, Y.-C. Liang, J. Chen, and E. G. Larsson, "Weighted sum-rate maximization for reconfigurable intelligent surface aided wireless networks," *IEEE Trans. Wireless Commun.*, vol. 19, no. 5, pp. 3064–3076, 2020.
- [9] X. Yu, D. Xu, and R. Schober, "MISO wireless communication systems via intelligent reflecting surfaces: (invited paper)," in *2019 IEEE/CIC International Conference on Communications in China (ICCC)*, 2019, pp. 735–740.

- [10] S. Zhang and R. Zhang, "Capacity characterization for intelligent reflecting surface aided MIMO communication," *IEEE J. Sel. Areas Commun.*, vol. 38, no. 8, pp. 1823–1838, 2020.
- [11] C. Pan, H. Ren, K. Wang, W. Xu, M. ElKashlan, A. Nallanathan, and L. Hanzo, "Multicell MIMO communications relying on intelligent reflecting surfaces," *IEEE Trans. Wireless Commun.*, vol. 19, no. 8, pp. 5218–5233, 2020.
- [12] C. Huang, A. Zappone, G. C. Alexandropoulos, M. Debbah, and C. Yuen, "Reconfigurable intelligent surfaces for energy efficiency in wireless communication," *IEEE Trans. Wireless Commun.*, vol. 18, no. 8, pp. 4157–4170, 2019.
- [13] J. Yuan, Y.-C. Liang, J. Joung, G. Feng, and E. G. Larsson, "Intelligent reflecting surface-assisted cognitive radio system," *IEEE Trans. Commun.*, vol. 69, no. 1, pp. 675–687, 2021.
- [14] C. Cai, H. Yang, X. Yuan, Y.-J. A. Zhang, and Y. Liu, "Reconfigurable intelligent surface assisted D2D underlay communications: A two-timescale optimization design," *J. Commun. Inf. Netw.*, vol. 5, no. 4, pp. 369–380, 2020.
- [15] T. Hou, Y. Liu, Z. Song, X. Sun, Y. Chen, and L. Hanzo, "Reconfigurable intelligent surface aided NOMA networks," *IEEE J. Sel. Areas Commun.*, vol. 38, no. 11, pp. 2575–2588, 2020.
- [16] H. Liu, X. Yuan, and Y.-J. A. Zhang, "Reconfigurable intelligent surface enabled federated learning: A unified communication-learning design approach," *IEEE Trans. Wireless Commun.*, vol. 20, no. 11, pp. 7595–7609, 2021.
- [17] Z. Zhang and L. Dai, "A joint precoding framework for wideband reconfigurable intelligent surface-aided cell-free network," *IEEE Trans. Signal Process.*, vol. 69, pp. 4085–4101, 2021.
- [18] W. Tang, M. Z. Chen, X. Chen, J. Y. Dai, Y. Han, M. Di Renzo, Y. Zeng, S. Jin, Q. Cheng, and T. J. Cui, "Wireless communications with reconfigurable intelligent surface: Path loss modeling and experimental measurement," *IEEE Trans. Wireless Commun.*, vol. 20, no. 1, pp. 421–439, 2021.
- [19] Y. Yang, B. Zheng, S. Zhang, and R. Zhang, "Intelligent reflecting surface meets OFDM: Protocol design and rate maximization," *IEEE Trans. Commun.*, vol. 68, no. 7, pp. 4522–4535, 2020.
- [20] B. Zheng and R. Zhang, "Intelligent reflecting surface-enhanced OFDM: Channel estimation and reflection optimization," *IEEE Wireless Commun. Lett.*, vol. 9, no. 4, pp. 518–522, 2020.
- [21] Z. Mao, W. Wang, Q. Xia, C. Zhong, X. Pan, and Z. Ye, "Element-grouping intelligent reflecting surface: Electromagnetic-compliant model and geometry-based optimization," *IEEE Trans. Wireless Commun.*, pp. 1–1, 2022.
- [22] C. Cai, X. Yuan, W. Yan, Z. Huang, Y.-C. Liang, and W. Zhang, "Hierarchical passive beamforming for reconfigurable intelligent surface aided communications," *IEEE Wireless Commun. Lett.*, vol. 10, no. 9, pp. 1909–1913, 2021.
- [23] M. Najafi, V. Jamali, R. Schober, and H. V. Poor, "Physics-based modeling and scalable optimization of large intelligent reflecting surfaces," *IEEE Trans. Commun.*, vol. 69, no. 4, pp. 2673–2691, 2021.
- [24] A. Khaleel and E. Basar, "A novel NOMA solution with RIS partitioning," *IEEE J. Sel. Top. Signal Process.*, pp. 1–1, 2021.
- [25] 3GPP, "Study on channel model for frequencies from 0.5 to 100 GHz (3GPP TR 38.901 version 16.1.0 release 16)," 2019. [Online]. Available: https://www.3gpp.org/ftp/Specs/archive/38_series/38.901/38901-g10.zip
- [26] A. Schrijver, *Theory of linear and integer programming*. John Wiley & Sons, 1998.
- [27] A. Goldsmith, *Wireless communications*. Cambridge university press, 2005.
- [28] Ö. Özdoğan, E. Björnson, and E. G. Larsson, "Intelligent reflecting surfaces: Physics, propagation, and pathloss modeling," *IEEE Wireless Commun. Lett.*, vol. 9, no. 5, pp. 581–585, 2019.
- [29] J. J. Moré, "The levenberg-marquardt algorithm: implementation and theory," in *Numerical analysis*. Springer, 1978, pp. 105–116.
- [30] Q. Shi, M. Razaviyayn, Z.-Q. Luo, and C. He, "An iteratively weighted MMSE approach to distributed sum-utility maximization for a MIMO interfering broadcast channel," *IEEE Trans. Signal Process.*, vol. 59, no. 9, pp. 4331–4340, 2011.